Journal of South American Earth Sciences xxx (2011) 1–23

Contents lists available at ScienceDirect

Journal of South American Earth Sciences

journal homepage: www.elsevier.com/locate/jsames

Petrology and SHRIMP U–Pb zircon geochronology of Cordilleran granitoids of the Bariloche area, Argentina

A. Castro [a,*], I. Moreno-Ventas [a], C. Fernández [b], G. Vujovich [c], G. Gallastegui [d], N. Heredia [d], R.D. Martino [e], R. Becchio [f], L.G. Corretgé [g], J. Díaz-Alvarado [b], P. Such [h], M. García-Arias [g], D.-Y. Liu [i]

[a] Departamento de Geología, Universidad de Huelva, Campus del Carmen, 21071 Huelva, Spain
[b] Departamento de Geodinámica y Paleontología, Universidad de Huelva, Spain
[c] Laboratorio de Tectónica Andina, FCEN, Universidad de Buenos Aires/CONICET, Argentina
[d] Instituto Geológico y Minero de España (IGME), Oviedo, Spain
[e] Cátedra de Tectónica, Universidad Nacional de Córdoba/CONICET, Argentina
[f] Departamento de Geología, Universidad Nacional de Salta/CONICET, Argentina
[g] Departamento de Geología, Universidad de Oviedo, Spain
[h] Facultad de Ciencias Naturales, Universidad Nacional de Tucumán/CONICET, Argentina
[i] Beijing SHRIMP Center, Chinese Academy of Geological Sciences, Beijing, PR China

ARTICLE INFO

Article history:
Received 31 May 2010
Accepted 2 March 2011

Keywords:
Cordilleran granites
Batholith
Patagonian batholith
Andes
Granodiorite
Tonalite
Jurassic

ABSTRACT

A petrological and geochronological study of Cordilleran granitoid intrusions in the Bariloche area (Argentina) point to a complex time-compositional evolution of magmatic processes in relation with oblique subduction of the Phoenix plate below the South America active margin during Jurassic times. The observed geochemical variations in both major and trace elements, together with the textural and mineralogical relations, point to a roughly defined, overall process of magmatic "filtering" linking all the intrusive batholithic rocks of the Bariloche area. These data suggest that the composition of the parental magma that underwent fractionation may be an intermediate magma with SiO_2 = 58–60 wt%, MgO = 2.5 wt%, FeO = 6.5 wt%, CaO = 6.1. These are coincident with the typical compositions of evolved andesites. Magnetite, amphibole and plagioclase are the main phases involved in the fractionation process. According to Hbl thermobarometry, fractionation may have taken place, at least in part, at shallow pressures (P = 0.5–1.5 kbar), possibly at the level of emplacement. The coupled observations of the two pressure dependent ratios, namely Sr/Y and La/Yb are pointing to a low-pressure, low-temperature final fractionation dominated by only Pl. The geochronologic study by U–Pb SHRIMP zircon determinations of 14 samples from granites, tonalites and diorites yield a broad range of about 20 Ma, between 150 and 170 Ma at the Medium Jurassic. The batholith was accomplished by a protracted magmatic activity that lasted for about 20 Ma. This time is much longer than the time elapsed from intrusion to complete crystallization of shallow magma chambers. It is concluded that amalgamation of discrete magma pulses is the dominant process that built-up the batholith. The observed structures suggest that the fractures conditioning the emplacement of the magma batches were arranged en échelon and show a right-stepping. The resulting geometry is compatible with the activity of a large-scale, sinistral, N–S trending, strike-slip fracture zone permitting the emplacement of each magma pulse. This major, strike-slip fault system should be deeply entrenched in the crust to allow intruding magmas generated and fractionated at depth. Because batholith generation is a direct consequence of subduction, structural relations and ages can be used to constraint the plate motion relations during Jurassic in this region of the South America active margin.

1. Introduction

It is broadly recognized that batholiths supply relevant information about lithosphere evolution in relation with subduction in active continental margins (Lee et al., 2007; Silver and Chappell, 1988; Wyllie, 1977). On one hand, batholiths represent large mass transfer processes from deep zone of the lithosphere to the upper continental crust, contributing to the conformation of the continental masses (Hawkesworth and Kemp, 2006). On the other hand, batholith magma generation needs special thermal regimes in the crust and mantle, which require particular geodynamic processes

* Corresponding author.
E-mail address: dorado@uhu.es (A. Castro).

0895-9811/$ – see front matter © 2011 Elsevier Ltd. All rights reserved.
doi:10.1016/j.jsames.2011.03.011

(Annen et al., 2006a, 2006b; DeCelles et al., 2009). Furthermore, batholiths transport inherited geochemical fingerprints from their source, which may be used to assess the relative contribution from continental crust, subducted oceanic crust or mantle wedge in their generation, which can be used to constraint source composition and depth of magma generation (Kemp and Hawkesworth, 2003).

The possibility of getting precise age determinations by U–Pb zircon geochronology in batholiths, allows us to establish a precise chronology of the thermal and geodynamic processes associated with the generation of magmas. Consequently, batholiths are among the most important geologic sources of information in orogenic environments. In this sense, Cordilleran batholiths formed along the continental margin of the Americas have received special attention along the last years with the aim of constraining the time-evolution of the subduction system. Detailed and comprehensive studies have been carried out in North America (Crawford et al., 2005; Lackey et al., 2005; Lee et al., 2007; Valencia-Moreno et al., 2003) and South America (Hervé et al., 2007; Pankhurst et al., 1999; Parada et al., 1999). Although these studies can be considered as a first-order approach to constrain the relation between subduction and magma generation in active continental margins, it is clear that they have contributed largely to a better understanding the complex processes involved.

In South America, the Mesozoic-Tertiary Patagonian batholith, extending for more than 3000 km from 39° to 55° S latitude, and the Coast batholith of Northern Chile, from 33° to 38° S latitude, is among the best examples in the world to develop geodynamic models in relation with subduction at active continental margins. The sporadic, but regular and almost continuous, production of magma for time-periods of about 150 Ma in South Patagonia (Hervé et al., 2007) and for about 200 Ma in Coast Chile batholith (Parada et al., 1999), without the intervening action of accreted continental blocks, makes this sector of the America's margin of special interest to develop predictive models. The aim is to produce models for granite magma generation in continental margins that can be applied in more complex regions and ancient orogenic belts in which subduction was followed by continental collision (e.g. the Thethyan orogenic belt in Asia). Consequently, the Cordilleran batholiths of the South American continent can be used as a natural laboratory in which geodynamic models supplied by both empirical formulations based on geological-geophysical data (Collins, 2002; DeCelles et al., 2009) and thermo-mechanical numerical experiments (Currie et al., 2007; Gerya et al., 2004; Vogt et al., 2009) and phase equilibria determinations (Castro et al., 2010; Castro and Gerya, 2008) can be tested by means of a combination of structural, geochronological and petrological studies.

In spite of the valuable information supplied by previous studies of these Andean batholiths in South America, our knowledge is still limited and important areas still require detailed geochronological and petrological studies. We show in this paper new geochronologic and geochemical data of granodiorite-tonalite intrusions from one of these poorly known areas: the region of Bariloche in Argentina in the provinces of Río Negro and Neuquén (40°–42° S latitude). In addition, the confluence in this region of other large batholiths, the Subcordilleran plutonic belt and the Central Patagonian batholith (Rapela et al., 2005), which is linked to a process of Late Triassic-Early Jurassic subduction, highlights the special interest of the Bariloche area. In the study of the Bariloche region shown in this paper, precise U–Pb SHRIMP zircon ages are used to correlate large-scale processes of magma production in the continental crust or the lithospheric mantle with tectonic processes related to plate convergence and subduction. The data confirm the peculiarity of this batholithic sector. These are discussed in terms of correlation with neighboring batholithic masses with similar ages to the South and North along the active continental margin during large periods of the Mesozoic.

2. Geology and previous geochronology of the Bariloche region

The Bariloche region forms part of the Argentinean Patagonian Andes in the sector between 40°S and 42°S. The region is characterized by a poly-orogenic evolution with a Paleozoic Gondwanan basement, deformed during the Carboniferous and Permian times, covered by Mesozoic and Cenozoic rocks that were deformed by the Andean compression during the Cenozoic. Granitoid calc-alkaline magmatism is widespread, represented in the region by large plutonic bodies of supposed Mesozoic age. Small Tertiary granite intrusions are also present in the area.

The Mesozoic-Cenozoic rocks of the Andean cycle unconformably overlie the Gondwanan basement. The stratigraphic record starts with the deposition of a thick volcano-sedimentary series during the Lower Jurassic (Lizuaín, 1980), in relation with extensional tectonic setting (Giacosa and Heredia, 2001). Activity along N–S-trending normal faults conditioned the generation of tectonically controlled basins (grabens) to the west of the studied zone, where the volcano-sedimentary sequence was deposited. During the same age (185–195 Ma), the eastern part of the studied area remained as a relatively elevated region (horst), dominated by the intrusion of calc-alkaline granitoid plutons of the Subcordilleran plutonic belt (Rapela et al., 2005). This extensional episode was still active from the Middle Jurassic to the Cretaceous, with the intrusion of the huge Cordilleran batholith (Giacosa and Heredia, 2001) and the sedimentation of sedimentary rocks in the eastern part. The Andean compressional phases were responsible for the inversion of the Mesozoic extensional structures. A continental retroarc foreland basin (Ñirihuau Basin) was located at the front of the fold and thrust belt and progressively migrated eastward (Giacosa and Heredia, 2004).

The tectonostratigraphic data show that the Andean compression took place during, at least, three main stages: Upper Cretaceous-Paleocene (Ramos, 1999) not represented in this area, Middle Eocene to Early Oligocene, and Late Oligocene to the Miocene-Pliocene limit (Giacosa et al., 2005). These compressional periods alternated with extensional episodes when thick volcanic and volcano-clastic sequences were deposited.

The large Mesozoic granitoid plutons, which were emplaced during protracted extensional episodes, are the objective of this study. These are assumed part of the Patagonian batholith, which extends for more than 3000 km south of the Bariloche region along the coast of Chile. Previous geochronology data of the Patagonian batholith in the Bariloche region were reported by Toubes and Spikermann (1973), González Díaz (1982), Ramos et al. (1982) and Rapela et al. (1987). These refer to K–Ar and Rb–Sr ages of Late Jurassic to Miocene granitoids (150–8 Ma), although González Díaz (1982) dated a Middle Jurassic granitoid (172 ± 10 Ma) at Cerro Coihue, to the west of San Carlos de Bariloche. More precise is the geochronological information of the Subcordilleran plutonic belt, with zircon U–Pb ages ranging from 181 to 226 Ma in the Bariloche region (Varela et al., 2005; Rapela et al., 2005). K–Ar and Rb–Sr ages of the Subcordilleran granitoids vary from 177 to 10 Ma (e.g. Franchi and Page, 1980; Lizuaín, 1981; Rapela et al., 1987). Plutons belonging to the Central Patagonian batholith in the Bariloche region have been dated between 220 and 162 Ma (Rb–Sr, K–Ar; e.g. Varela et al., 1991; Rapela et al., 1992) and a precise U–Pb determination yielded 221 ± 3 Ma (Rapela et al., 2005). These previous geochronological data are summarized in Table 1. Given the scarcity of reliable geochronological data for the North Patagonian batholith in Argentina, this work presents the results of a project of sensitive high-resolution ion microprobe U–Th–Pb age determinations on zircons from Cordilleran granitoids of the Bariloche region.

Please cite this article in press as: Castro, A., et al., Petrology and SHRIMP U–Pb zircon geochronology of Cordilleran granitoids of the Bariloche area, Argentina, Journal of South American Earth Sciences (2011), doi:10.1016/j.jsames.2011.03.011

Table 1
Previous geochrological data of Mesozoic-Cenozoic granitoids of the Bariloche region between 40 and 44° S latitude.

	Patagonian batholith				Subcordilleran belt				Central patagonian batholith			
	Locality	Age	Rock	Ref.	Locality	Age	Rock	Ref.	Locality	Age	Rock	Ref.
Miocene	Brazo de la Tristeza	8 ± 0.4 (K–Ar)	Grd	1	Cerro Catedral	10 ± 0.5 (K–Ar)	Gr	1				
	Hoyada del Cerro López	9 ± 0.5 (K–Ar)	Grd	1	Cerro Catedral	13 ± 1 (K–Ar)	Gr	3				
	South of Cerro Tronador	15 ± 2 (K–Ar)	Grd	2								
Oligoceno	South of Cerro Tronador	24 ± 10 (K–Ar)	Grd	4								
Eocene	Cerro El Fuerte	51 ± 10 (K–Ar)	Grd	2	Arroyo Golondrina (Río Foyel)	46 ± 4 (K–Ar)	Grd	5				
	Lago Martín	53 ± 5 (K–Ar)	Grd	2	Arroyo Golondrina (Río Foyel)	55 ± 5 (K–Ar)	Grd	5				
					Río Villegas	51 ± 10 (K–Ar)	Grd	5				
					Lago Puelo	42 ± 2 (K–Ar)	Grd	6				
					Cordón Cholila	37 ± 2 (K–Ar)	Grd	6				
Late Cretaceous	Lago Perito Moreno	92 ± 10 (K–Ar)	Grd	3	Cerro Morrudo	82 ± 3 (K–Ar)	Grd	5				
	Lago Perito Moreno	93 ± 10 (Rb–Sr)	Grd	4								
	South of Cerro Tronador	71 ± 1 (K–Ar)	Grd	4								
	South of Cerro Tronador	79 ± 9 (K–Ar)	Grd	2								
Early Cretaceous	Lago Perito Moreno	112 ± 5 (K–Ar)	Grd	3	Río Villegas	102 ± 5 (K–Ar)	Grd	3				
	Lago Perito Moreno	131 ± 10 (K–Ar)	Grd	3	SW of Cerro Catedral	113 ± 7 (K–Ar)	Grd	3				
	South of Cerro Tronador	102 ± 10 (K–Ar)	Grd	3	Lago Mascardi	127 ± 10 (K–Ar)	Gd	3				
	South of Cerro Tronador	113 ± 2 (K–Ar)	Grd	4	Lago Gutiérrez	140 ± 6 (K–Ar)	Gd	7				
	Lago Steffen	103 ± 5 (K–Ar)	Grd	2	Cerro Piltriquitrón	130 ± 10 (K–Ar)	Grd	5				
	Lago Escondido	100 ± 5 (K–Ar)	Grd	2	Epuyén-El maitén	109 ± 5 (K–Ar)	Grd	6				
	Veranadas de Tillería	124 ± 5 (K–Ar)	Grd	2	Epuyén-El maitén	104 ± 5 (K–Ar)	Grd	6				
	Arroyo Motoco	123 ± 5 (K–Ar)	Grd	2	Leleque	141 ± 5 (K–Ar)	Gr	8				
Late Jurassic	Cerro Negro	150 ± 10 (K–Ar)	Grd	2								
Middle Jurassic	Cerro Coihue	172 ± 10 (K–Ar)	Grd	2	Leleque	164 ± 4 (Rb–Sr)	Gr	9	Paso de las Flores-Comallo	171 (Rb–Sr)	To	11
					Lago Puelo	173 ± 10 (K–Ar)	To	6	Sañicó	162 ± 7 (K–Ar)	Ga	11
					Cruce Meliquina	172 ± 15 (K–Ar)	Gd	7	Sañicó	170 ± 6 (K–Ar)	Ga	11
					José de San Martín	167 ± 30 (K–Ar)	Grd	10	Sañicó	163 ± 5 (K–Ar)	Ga	11
									Escuela Merino	171 (Rb–Sr)	To	11
									Río Chico, C. Angostura	174 ± 5 (K–Ar)	Gd	7
									Pilahué	170 (K–Ar)	Dt/Ga	12
Early Jurassic					Lago Puelo	177 ± 5 (K–Ar)	Dt	6	Pilcaniyeu	186 ± 4 (Rb–Sr)	Grd	17
					La Angostura	183 ± 13 (Rb–Sr)	Gr	13				
					Arroyo La Tuerta	200 ± 24 (Rb–Sr)	Gd	13				
					José de San Martín	197 ± 10 (K–Ar)	Grd	10				
					José de San Martín	182 ± 2 (U–Pb)	Q-Md	14				
					Aleusco	180 ± 10 (K–Ar)	Grd	15				
					Aleusco	177 ± 6 (K–Ar)	Grd	16				
					Aleusco	179 ± 7 (K–Ar)	Grd	16				
					Aleusco	184 ± 6 (K–Ar)	Grd	16				
					Aleusco	185 ± 2 (U–Pb)	Gd	14				
					La Angostura	181 ± 2 (U–Pb)	Gr	14				
					Leleque	181 ± 3 (U–Pb)	Gd	14				
Late Triassic					Lago Gutiérrez	226 ± 17 (U–Pb)	Gd	7	Mencué-Chasicó	210 ± 9 (Rb–Sr)	Grd	18
					José de San Martín	206 ± 10 (K–Ar)	Ga	10	Gastre zone	220 ± 3 (Rb–Sr)	Grd	19
					José de San Martín	207 ± 10 (K–Ar)	Grd	10	Lipetrén	208 ± 1 (Rb–Sr)	Grd	19
					José de San Martín	211 ± 10 (K–Ar)	Ga	10	Gastre zone	221 ± 3 (U–Pb)	Grd	14

Name of batholiths and magmatic belt from Rapela et al. (2005). Data sources: 1. Rapela et al. (1987), 2. González Díaz (1982), 3. Toubes and Spikermann (1973), 4. González and Valvano (1979), 5. González Díaz and Lizuaín (1984), 6. Lizuaín (1981), 7. Varela et al. (2005), 8. Lizuaín (1983), 9. Rapela (1999), 10. Franchi and Page (1980), 11. Varela et al. (1991), 12. Cucchi (1991), 13. Gordon and Ort (1993), 14. Rapela et al. (2005), 15. Spikermann et al. (1988), 16. Haller et al. (1999), 17. Alonso (1990) in Rapela and Alonso (1991), 18. Cingolani et al. (1991), 19. Rapela et al. (1992). Grd: Granitoids, Gr: Granite, Gd: Granodiorite,To: Tonalite, Q-Md: Quartz-Monzodiorite, Dt: Diorite, Ga: Gabbro. Age scale compiled by Walker and Geiissman (2009).

Please cite this article in press as: Castro, A., et al., Petrology and SHRIMP U–Pb zircon geochronology of Cordilleran granitoids of the Bariloche area, Argentina, Journal of South American Earth Sciences (2011), doi:10.1016/j.jsames.2011.03.011

3. Analytical techniques

About 110 samples were collected from plutonic rocks of the Bariloche region. A set of 37 fresh samples was selected for major and trace element analyses (Table 2). Major elements and Zr were analyzed by X-Ray fluorescence (XRF) at the University of Oviedo (Spain) using glass beads. Precision of the XRF technique was better than ± 1.5% relative. Trace element and rare earth elements (REE) were analyzed by inductively coupled plasma mass spectrometry (ICP-MS) with an HP-4500 system at the University of Huelva, following digestion in a HF + HNO_3 (8:3) solution, drying and second dissolution in 3 ml HNO_3. The average precision and accuracy for most of the elements were controlled by repeated analyses of SARM-1 (granite) and SARM-4 (norite) international rock standards. They fall in the range of 5–10% relative. Probe analyses were obtained with a JEOL JXA-8200 SuperProbe at the University of Huelva. A combination of silicates and oxides were used for calibration.

A set of 14 representative samples was processed for zircon separation and U–Pb geochronology. This first sampling shown in this paper is focused on the granitoid rocks that form the large plutonic intrusions in the Bariloche region. The aim of the SHRIMP

Table 2
Whole-rock analyses of major and trace elements of representative granitoid rocks of the Bariloche region.

Rock type	Diorite	Diorite	Qtz-diorite	Qtz-diorite	Tonalite-granodiorite	Tonalite-granodiorite	Granite	Granite	Granite	Granite	Granite	Granite
Sample	A-208-8	A-208-29	A-208-14	A-208-11	A-208-22	A-208-6	A-208-20	A-208-13	A-208-31	A-208-33	A-208-1	A-208-48
(wt.%)												
SiO_2	50.71	56.14	60.98	62.48	69.74	71.32	71.64	71.80	74.30	74.50	75.66	77.55
TiO_2	1.17	1.16	0.88	0.75	0.44	0.35	0.41	0.39	0.26	0.18	0.15	0.13
Al_2O_3	16.73	17.37	16.79	16.29	15.05	14.11	13.88	14.10	13.97	14.09	13.20	12.58
FeOt	7.58	7.33	5.90	5.83	3.09	2.98	2.69	2.71	1.93	1.80	1.40	1.55
MgO	5.28	2.54	2.29	2.09	0.99	0.88	0.56	0.50	0.36	0.31	0.31	0.08
MnO	0.15	0.21	0.12	0.11	0.07	0.07	0.06	0.06	0.03	0.07	0.04	0.03
CaO	9.10	6.66	5.10	6.17	3.14	3.30	1.57	2.02	1.83	1.54	0.64	0.71
Na_2O	2.55	2.48	2.84	2.67	3.39	3.10	3.26	3.01	3.11	3.15	2.77	3.38
K_2O	1.27	1.85	2.00	1.33	2.37	1.79	4.16	4.03	3.36	3.41	4.57	3.62
P_2O_5	0.13	0.27	0.23	0.13	0.13	0.07	0.08	0.08	0.06	0.08	0.06	0.02
Loi	3.50	2.85	1.82	0.91	0.90	1.39	1.20	0.72	0.64	0.70	0.93	0.15
Total	98.17	98.85	98.95	98.76	99.31	99.34	99.52	99.40	99.83	99.81	99.73	99.79
Mg#[a]	0.55	0.38	0.41	0.39	0.36	0.34	0.27	0.25	0.25	0.24	0.28	0.08
ASI[b]	0.76	0.97	1.06	0.96	1.10	1.09	1.10	1.09	1.16	1.22	1.25	1.17
(ppm)												
Li	25.14	14.92	18.15	7.79	7.94	8.82	23.31	30.52	4.52	38.09	14.96	5.64
Be	0.83	1.25	1.85	0.91	1.86	1.04	1.83	1.90	2.08	2.05	1.91	1.57
Sc	41.19	29.49	12.96	26.17	11.81	10.93	4.24	6.71	8.03	0.00	2.53	5.58
V	225.2	177.2	125.6	152.8	55.80	56.94	27.80	31.27	19.97	12.81	12.35	7.45
Cr	288.2	129.1	148.6	152.4	143.1	116.4	136.0	170.8	147.6	156.9	147.7	218.4
Co	30.91	16.62	14.53	14.83	5.86	5.90	3.47	4.17	3.11	1.71	1.62	1.01
Ni	36.19	9.86	112.7	8.83	4.78	4.93	3.50	4.01	2.94	89.57	3.02	4.38
Cu	23.65	20.86	19.33	34.76	3.23	4.79	15.43	6.22	2.34	1.61	2.08	5.71
Zn	76.61	178.4	78.33	54.39	36.80	83.27	53.22	30.12	14.98	17.29	20.38	9.79
Ga	16.51	19.54	20.11	16.57	17.32	14.12	16.02	16.09	15.15	14.40	15.69	16.64
Rb	50.97	50.57	74.15	42.98	61.24	38.66	170.2	155.0	91.95	116.2	198.5	86.29
Sr	341.3	473.0	378.3	314.6	294.1	273.9	145.8	161.0	187.8	149.7	93.67	46.96
Y	17.79	28.95	28.46	32.19	16.59	15.10	39.11	30.49	21.72	9.57	13.43	31.10
Zr	28.73	6.76	21.62	7.83	24.12	0.95	45.23	22.47	2.73	14.63	31.28	7.18
Nb	3.79	5.99	9.38	4.16	7.74	2.98	10.82	9.19	7.43	7.01	11.03	7.48
Cs	3.74	0.80	2.34	2.21	1.48	1.19	5.54	5.44	1.42	3.27	3.68	0.31
Ba	283.9	617.8	492.3	323.4	650.0	640.5	756.0	702.3	690.8	648.9	519.6	889.4
La	11.80	20.60	27.65	17.33	26.18	13.29	39.10	27.68	36.23	19.41	33.35	31.11
Ce	23.87	46.75	59.79	39.23	50.13	26.42	83.01	59.16	72.32	37.72	68.80	62.87
Pr	2.91	6.20	7.50	5.33	5.63	3.07	10.10	7.38	8.10	4.36	7.95	7.76
Nd	13.40	25.50	30.42	24.91	20.14	11.66	39.45	29.07	29.50	14.90	28.72	30.51
Sm	3.42	6.12	6.46	5.91	3.53	2.78	8.31	6.40	5.55	2.80	5.91	6.44
Eu	1.19	1.73	1.64	1.22	0.90	0.70	1.25	1.26	0.94	0.59	0.52	0.93
Gd	3.54	5.88	5.83	5.43	3.11	2.42	7.02	5.80	4.38	2.19	4.22	5.81
Tb	0.57	0.91	0.95	0.96	0.53	0.51	1.18	0.93	0.73	0.36	0.62	0.99
Dy	3.33	5.10	5.20	5.40	2.98	2.38	6.19	5.30	3.49	1.75	2.91	5.48
Ho	0.73	1.20	1.06	1.24	0.58	0.57	1.42	1.20	0.76	0.35	0.48	1.18
Er	1.91	2.96	2.80	3.18	1.54	1.73	3.82	3.08	2.18	0.90	1.24	2.94
Tm	0.37	0.49	0.42	0.50	0.28	0.27	0.55	0.40	0.33	0.16	0.18	0.41
Yb	1.71	2.75	2.72	3.31	1.70	2.00	3.55	3.11	2.45	0.98	1.12	2.52
Lu	0.24	0.41	0.38	0.50	0.24	0.25	0.50	0.45	0.31	0.13	0.20	0.38
Hf	1.28	0.42	1.14	0.53	1.07	0.21	1.96	1.14	0.15	0.61	1.30	0.45
Ta	0.37	0.50	0.72	0.30	0.34	0.28	0.84	0.95	0.66	0.81	1.29	0.22
Pb	5.60	17.13	15.07	6.76	8.58	10.74	21.35	14.37	8.69	16.00	23.18	5.87
Th	4.38	5.91	7.87	3.65	8.03	4.20	16.84	13.27	12.76	9.12	17.89	11.13
U	0.79	0.70	1.63	0.80	1.53	1.19	2.21	2.08	1.14	1.38	3.05	1.59
ΣREE	68.99	126.6	152.8	114.5	117.5	68.04	205.5	151.2	167.3	86.61	156.2	159.3
$^{206}Pb/^{238}U$ Age[c]	154.5	172.5	171	161.7	168.1	149.9	171.6	168.9	171	156.8	163.5	173.2

[a] Mg# = Mol MgO/(MgO + FeO).
[b] ASI = Mol Al_2O_3/(CaO + Na_2O + K_2O).
[c] Mean $^{206}Pb/^{238}U$ age in Ma.

Please cite this article in press as: Castro, A., et al., Petrology and SHRIMP U–Pb zircon geochronology of Cordilleran granitoids of the Bariloche area, Argentina, Journal of South American Earth Sciences (2011), doi:10.1016/j.jsames.2011.03.011

study is two-fold. On one hand, we aim to get precise ages of granite emplacement and crystallization. On the other hand, we plan to identify pluton-scale changes in relation with the sequence of magma pulses and possible zircon inheritances. Zircon separation was accomplished by traditional techniques using dense liquids and magnetic (Franz) separation. Selected crystals free of impurities and fractures were selected by hand-picking with a binocular lens. These were mounted in epoxy, together with reference standards, and polished. Sectioned zircons were studied by CL imaging for selection of point analyses. Core and rims were analyzed in several grains of each individual sample with the aim of identifying inherited cores. These selected points were target over the CL images and analyzed for U–Th–Pb isotopes with SHRIMP at the Beijing-SHRIMP Center (Chinese Academy of Geological Sciences, Beijing), following methods given in Williams (1998) and references therein. The data were processed with ISOPLOT software (Ludwig, 2003) for Concordia plots, probability density plots, stacked histograms and weighted means and Concordia age calculations.

4. Granite types and structures in the Bariloche area

4.1. Mapping and general structures

The studied zone includes a quadrangle of around 11,000 km^2, extending from 40°34′S to 42°00′S and from 71°00′W to 71°45′W in the Bariloche region of Argentina (Fig. 1). Large, N–S-directed Cenozoic reverse faults and thrusts and Mesozoic normal faults inverted during the Andean contractional episodes, are the main structures mapped in this region (Fig. 1). The trend of reverse faults and thrusts changes to NW–SE between San Carlos de Bariloche and Villa de la Angostura, to the north of the Nahuel-Huapi Lake. An eastward verging imbricate thrust system, probably diverging from a floor thrust, has been interpreted at San Carlos de Bariloche (Fig. 1, cross section I–I′), while a more complex structure, with triangle zones and pop-ups can be seen more to the south, at El Bolsón (Fig. 1, cross section II–II′). The thrusted blocks are composed of Paleozoic basement rocks, Early Jurassic volcanic and volcano-sedimentary rocks and granitoids of the Subcordilleran plutonic belt, granitoids of the Cordilleran batholith, and Cenozoic sedimentary and volcanic rocks. The Cordilleran granitoids mostly outcrop along a N–S belt covering the western half of the studied area, although their exposure widen eastwards to the north of San Carlos de Bariloche (Fig. 1). Accordingly, the studied area has been subdivided into a northern zone and a southern zone (Fig. 1). The Cordilleran granitoids intruded the rocks of the Paleozoic basement and the Early Jurassic volcanic and volcano-sedimentary series. The external contacts of the Cordilleran batholith are sub-vertical or inward dipping, and are NW–SE to NNW–SSE trending (Fig. 2i,j). Therefore, these contacts are oblique and systematically crosscut by the more recent, N–S oriented Cenozoic thrusts and reverse faults (Fig. 1). Internal contacts between distinct granitoid facies are commonly sharp, although smooth transitions have been occasionally observed. The size of the individual plutons inside the Cordilleran batholith is difficult to determine due to the scarcity of continuous exposures. However, when observed, individual plutons are sub-vertical tabular bodies, several tens to a few hundred meters in thickness, which coincides with the description made by Pankhurst et al. (1999) from the North Patagonian batholith in Aysén (Chile). The internal fabric of the Cordilleran granitoids is commonly planar (foliation) and defined by the preferred orientation of the long axes of euhedral or subhedral crystals of plagioclase and amphibole (see photomicrographs in Supplementary Material; Appendix A). This feature indicates that the observed foliation is magmatic in origin. Preferred orientation of the long axes of isolate, elongate mafic microgranular enclaves, alignment of mafic enclave corridors, and parallel arrangement of mafic schlieren also contribute to define this magmatic foliation, that is more strongly developed in the vicinity of pluton contacts. The average strike of the magmatic foliation is NW–SE to NNW–SSE (Fig. 2a–d), sub-parallel to the trend of the external contacts of the batholith. Interestingly, the main foliation of the Paleozoic basement shows a similar azimuth (Fig. 2g,h). In the northern zone, the magmatic foliation shows moderate to high dips to the NE (Fig. 2a). More variable dips have been measured at the southern zone (Fig. 2c), although a statistical predominance of moderately to highly SW-dipping planes is recognizable. Locally, in particular near the external contacts of the batholith, a solid-state fabric (foliation and lineation) can be observed. Quartz crystals are stretched and show blocky subgrains, with two orthogonal systems of subgrain boundaries, and polycrystalline quartz aggregates of equant grains probably developed by dynamic recrystallization. Plagioclase crystals are commonly fractured, although deformation twins and bent crystals with undulose extinction have also been observed (microphotograph in Supplementary Material; Appendix A). These microstructures in quartz and plagioclase are indicative of deformation temperatures around 400 °C or even higher (e.g. Passchier and Trouw, 1996). The spatial attitude of this solid-state foliation is similar to that of the magmatic foliation (Fig. 2g), with a NW–SE to NNW–SSE directed average azimuth (Fig. 2h). The measured lineations show contrasted plunges, although they share the same NW–SE trending azimuth (Fig. 2g). Kinematic criteria allow assigning a dextral rotation component to the deformation responsible for these solid-state fabrics. Finally, two sets of sub-vertical mafic dikes have been measured, NW–SE and E–W trending, respectively (Fig. 2k).

4.2. Rock type nomenclature and magmatic series definition

The large plutonic bodies mapped and sampled in the Bariloche region are dominantly composed of silicic rocks forming a continuous series from Qtz-diorites to tonalites, granodiorites and granites. More mafic, dioritic compositions are subordinate, representing less than 10 vol% of the outcropping rocks. With the exception of diorites, the other groups show gradual transitions over large distances in the field. It is impossible to trace lithological limits. However, in order to follow a systematic description, the rocks were initially classified by field and petrographic criteria based on the color index and feldspar mineralogy. Lately, this provisional classification was corrected by using chemical criteria that, in general terms follow the TAS classification diagram (Fig. 3a). Four large groups have been distinguished: (1) Hbl-diorite, (2) Qtz-diorite, (3) tonalite-granodiorite, and (4) granite. Rocks of the Hbl-diorite group (HD) have $SiO_2 < 60$ wt%, with CaO and FeO > 6 wt% typically and MgO in the range 3–5 wt%. Other geochemical features will be given later on in the paper. The second group is formed by Qtz-diorites (QD), which is defined by rocks having a silica range of 60–63 wt% SiO_2, for CaO and FeO > 5 wt%. The third and most abundant group, is formed by tonalites and granodiorites (TG) rocks with a silica range of 63–71 wt% SiO_2, for CaO and FeO > 3 wt%. These two rock types are considered together because the local changes in the Kfs content shift the classification without appreciable textural and color index changes. Finally, the group of granites (G) is defined for rocks with $SiO_2 > 71$ wt%, with typically FeO < 3 wt% and CaO < 2 wt%. The four groups show continuous and discontinuous geochemical variations that are analyzed in a later section with the aim of establishing genetic links, to identify magmatic processes and to constraint intensive parameters. These will give signification to radiometric ages in terms of thermal and tectonic evolution of the studied region.

Please cite this article in press as: Castro, A., et al., Petrology and SHRIMP U–Pb zircon geochronology of Cordilleran granitoids of the Bariloche area, Argentina, Journal of South American Earth Sciences (2011), doi:10.1016/j.jsames.2011.03.011

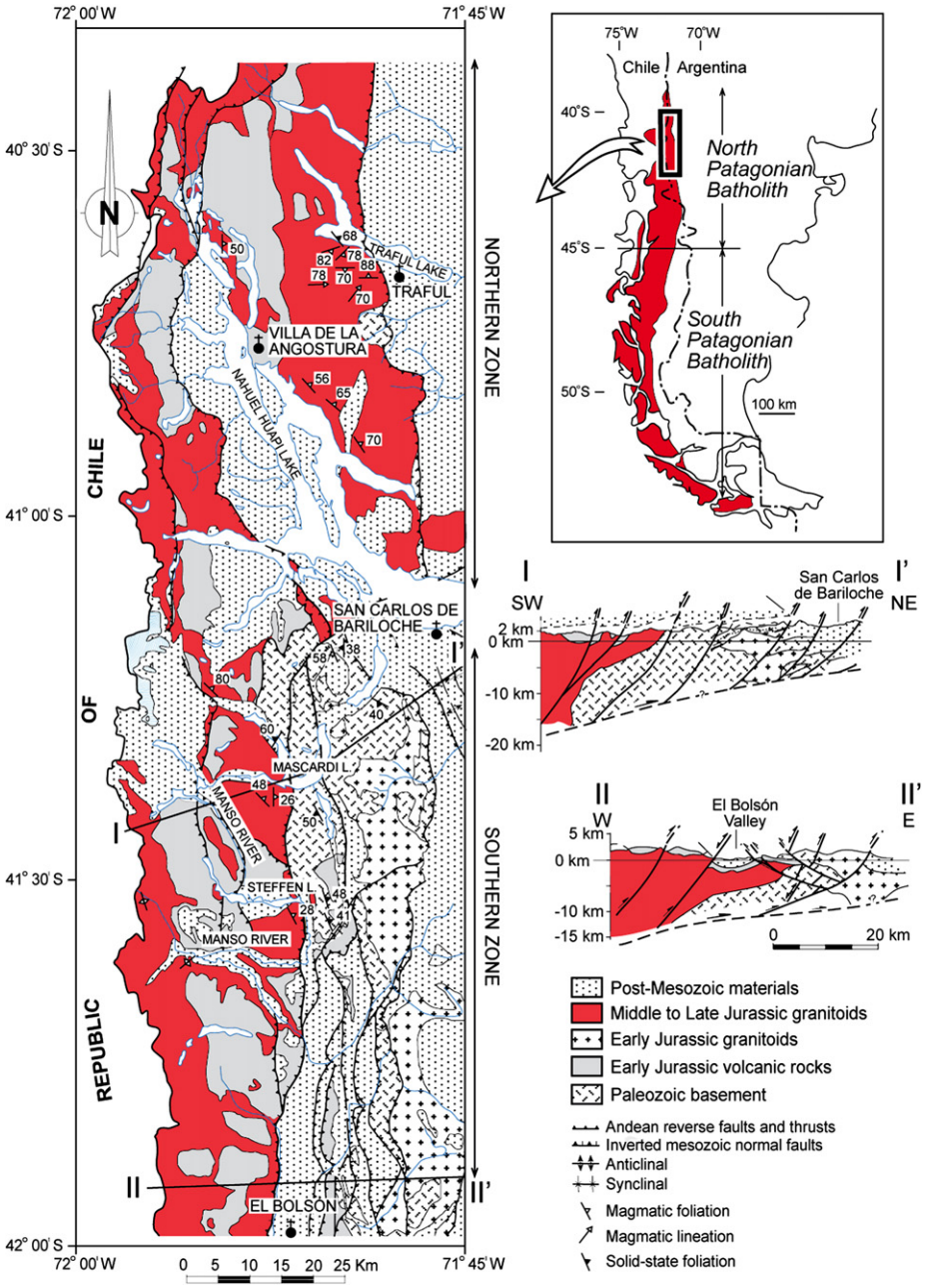

Fig. 1. Geological map of the Bariloche region. Inset shows its location inside the North Patagonian Batholith. The traces of cross sections I–I′ and II–II′ are indicated in the map. Modified from Giacosa and Heredia (2004), García-Sansegundo et al. (2009) and our own data.

Granitoids ($SiO_2 > 60$ wt%), which include QD, TG and G groups, define a good continuous calcic trend in the MALI (modified alkali-lime index; Frost et al., 2001) vs silica classification diagram (Fig. 4b). They are magnesian a calcic with ASI close to 1 [alumina saturation index, ASI = molar $Al_2O_3/Na_2O + K_2O+(CaO\text{-}1.67*P_2O_5)$]. Diorites plot in part in the calcic trend and part in the calc-alkalic trend in the same diagram. These features will be described later on in the paper. Here we show these diagrams only for purposes of rock classification and series characterization.

4.3. Petrography

Most plutonic rocks in the studied area are light-colored rocks of tonalite and granodioritic composition, showing coarse- to medium-grained igneous textures. Granites *s.s.* are more abundant at the northern part of the studied area, while diorites predominate southwards. Detailed descriptions, mineral compositions and photomicrographs of all these rocks are shown in the Supplementary Material (Appendix A). The diorite group (DG) is a homogeneous suite of hornblende ± biotite-diorites with pyroxene-hornblende facies located near the contacts and forming mafic microgranular enclaves. Dioritic enclaves show the typical features of local dissolution (García-Moreno et al., 2006). They are dark-grey colored, unequant, coarse- to fine-grained facies, showing a variety of textures from isotropic to foliate. Chilled-margin diorites and enclaves show cumulate foliate textures of Hbl + Mt ± Px ± Ol (mineral symbols after Kretz, 1983). Rocks with porphyritic texture have phenocrysts of Pl and Hbl. Textural relations suggest that plagioclase crystallized before amphibole. The dominant assemblage consists of Hbl, Pl, Mt, Qtz and Kfs. Accessory phases are Ap, Ilm, Ttn, Py and Zrn.

Please cite this article in press as: Castro, A., et al., Petrology and SHRIMP U–Pb zircon geochronology of Cordilleran granitoids of the Bariloche area, Argentina, Journal of South American Earth Sciences (2011), doi:10.1016/j.jsames.2011.03.011

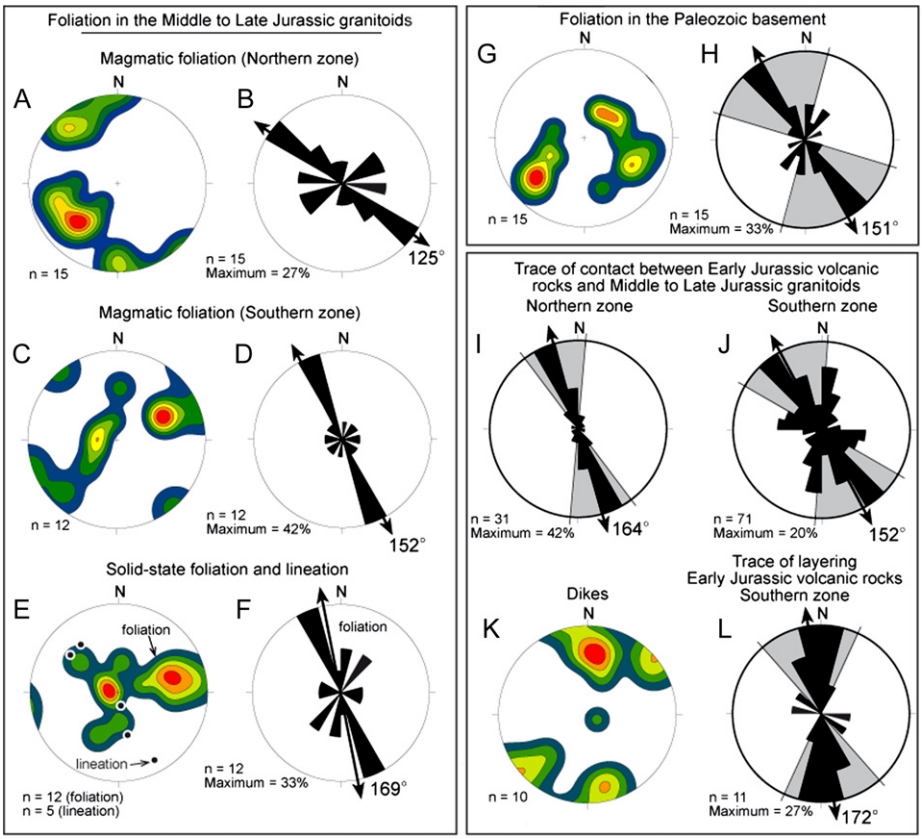

Fig. 2. Pole density diagrams and rose diagrams of the structural data measured in the Cordilleran granitoids and their host rocks. Density calculation: Gaussian, expected values under uniform distribution: 1σ. Equal area projection, lower hemisphere. Contour interval: 1σ. 15° classes (rose diagrams); double-headed arrow: mean circular direction; shaded area: confidence interval for a level of significance at the 5%. (a), (c), (e), (g), (k) Pole density diagrams of the magmatic foliation measured in the granitoids of the northern and southern zones, of the solid-state foliation, of the main foliation shown by the Paleozoic basement, and of mafic dikes, respectively. (b), (d), (f), (h), (i), (j), (l) Rose diagrams representing the azimuth of the magmatic foliation measured in the granitoids.

Amphibole is the main mafic mineral. It is present as green-pleochroic, subhedral/euhedral, porphyritic crystals (anhedral in the matrix). Most amphibole classify on the Leake et al. (1997) diagrams as Mg-hornblende [Si pfu = 6.55–7.15, $Mg/(Mg + Fe^{2+}) = 0.65–0.79$], and less abundantly as tschermakitic hornblende [Si pfu 6.48–6.44, $Mg/(Mg + Fe^{2+}) = 0.63$] and actinolitic hornblende [Si pfu = 7.45–7.50, $Mg/(Mg + Fe^{2+}) = 0.77–0.83$]. Plagioclase is present as euhedral/subhedral grains with oscillatory zoning ranging from An_{81} to An_{25}. Occasionally, it contains inclusions of primary Ep and Mt. Magnetite [$Cr/(Cr + Al) \approx 0.52$, $Fe^{2+}/(Fe^{2+} + Fe^{3+}) \approx 0.33$] is abundant in DG, mostly as inclusions in Hbl. Zircons are mainly included in Qtz, Pl, and occasionally in Hbl.

The assemblage of chilled-margin facies consists of porphyritic Pl laths (An_{64}), Cpx, primary Ep, Hbl, Mt and Qtz. The accessory assemblage consists of Ap, Mt and Zrn. Most Cpx classify as chrome-aluminian augite ($En_{47}Fs_{11}Wo_{42}$) and aluminian-diopside ($En_{40}Fs_{16}Wo_{44}$). Primary Ep appears abundantly in the matrix and occasionally as subhedral inclusions within Pl grains. Amphiboles classify as Mg-hornblende (Si pfu = 6.68, Mg# = 0.81) and Mg-hastingsite (Si pfu = 6.18, Mg# = 0.77). Plagioclase consists of a core (An_{65}) rimmed by a less calcic Pl (An_{10}). There are veins of Cc refilling interstices between euhedral Amph and Pl (<10%). Amphiboles from these veins are Mg-hornblende (Si pfu ≈ 6.96 and Mg# ≈ 0.68).

The quartz-diorite group (QDG) is a homogeneous suite of dark-grey, coarse- to medium-grained rocks that grade transitionally into diorites by increasing the relative contents of mafic minerals. Porphyritic facies present phenocrysts of Pl, and Amph and locally Bt. Some facies are porphyritic because the presence of poikocrystals of Qtz with inclusions of Amph, Bt and Pl. The dominant assemblage consists of Pl (andesine-labradorite), Amph (Mg-hornblende), Mg-rich Bt, Qtz and Kfs (rare). Accessory mineral assemblage consists of Mt, Ttn, Ilm, Zrn and heterogeneously disseminated Py. Epidote appears as primary as well as a secondary mineral. Amphibole is the main mafic mineral; it is present as green-pleochroic subhedral grains with weak patchy zoning. It appears as phenocrysts and as interstitial grains between plagioclase laths in the groundmass. Most amphiboles are Mg-hornblende (Si pfu = 7.0; Mg# = 0.70) and less abundantly tschermakitic hornblende (Si pfu = 6.42; Mg# = 0.83) and actinolitic hornblende (Si pfu = 7.28–7.35; Mg# = 0.70). Mica is present as brown-pleochroic, Mg-rich, anhedral grains (usually subhedral), ($Tc_3Ti\text{-}Phl_{17}Fe\text{-}East_{10}Mus_1East_{10}Phl_{53}$). It shows affinities with micas from calc-alkaline orogenic suites. Plagioclase shows a core with concentric oscillatory zoning, with bands of labradorite interspersed with An_{42}, rimmed by An_{24}. Zircon crystals are included in Qtz, Pl and Amph.

The Granodiorite-Tonalite Group (GTG) is a suite of grey, isotropic to foliate, coarse- to medium-grained rocks, ranging from porphyritic to glomeroporphyritic. The dominant assemblage consists of Amph, Bt, Pl, Qtz and Kfs. Accessory phases are Mt, Ap, Ttn, Ilm and Zrn. Amphibole and Bt are the main mafic minerals; they are present as phenocrysts of Amph and clots of Bt, and as part of the groundmass as anhedral grains between euhedral plagioclase laths. Amphibole is present as green-pleochroic subhedral to anhedral grains showing a weak patchy zoning. Most amphiboles

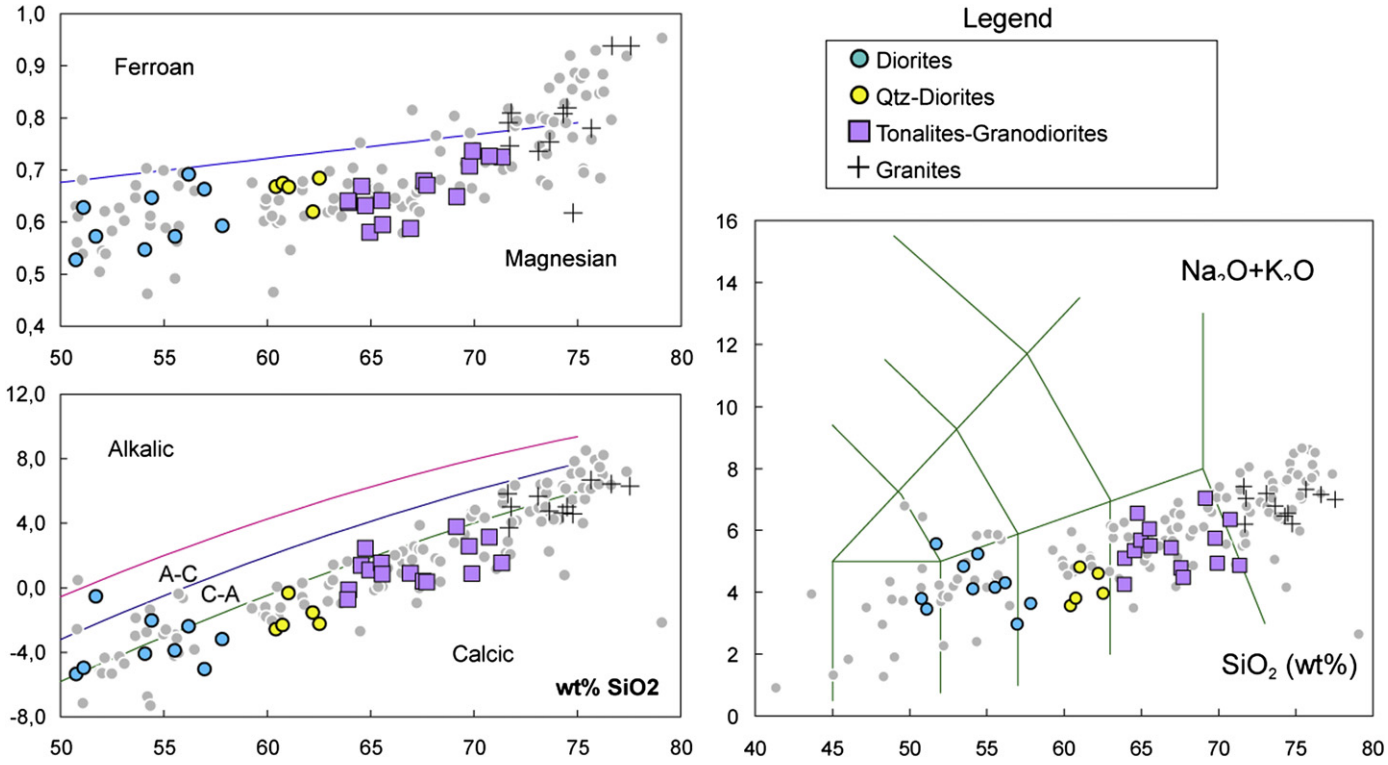

Fig. 3. General compositional features of granitoids and mafic rocks of the Bariloche region. (a) TAS (Total alkalis vs silica) classification diagram (Le Bas et al., 1986). (b) MALI-silica diagram (Frost et al., 2001). Grey dots correspond to data from the Patagonian batholith south of Bariloche (Data from Hervé et al., 2007; Pankhurst et al., 1999).

classify as Mg-hornblendes (Si pfu = 6.60–7.26; Mg# = 0.60–0.81). Biotite is present as brown-pleochroic subhedral grains with inclusions of Ap, Mt and Zrn. Most biotites show compositions around $Tc_5Ti\text{-}Phl_{16}Fe\text{-}East_{13}Mus_1East_{10}Phl_{53}$. Plagioclases show oscillatory zoning, ranging from An_{59} to An_9. Occasionally, plagioclases show a normal pattern of zoning consisting in a core of An_{47} rimmed by a band of An_{21}. Quartz and Kfs are the main felsic minerals of the groundmass. They have inclusions of Pl and Bt. Zircon appears as inclusions in Qtz, Bt and Kfs.

The Granite group (GG) is a suite of light-colored, coarse- to medium-grained, Bt-granites with textures ranging from porphyritic to glomeroporphyritic in a hypidiomorphic groundmass. The dominant assemblage consists of Bt, Pl, Kfs, Qtz, Ms and rarely, green Amph. Accessory phases are Mt, Ap, Ilm, Py and Zrn. Amphibole is present in some porphyritic facies forming euhedral phenocrysts and glomerules. Biotite is the main mafic mineral. It is present as brown-pleochroic anhedral grains, frequently embracing euhedral Pl grains. Most Bt has an end-member composition around $Tc_5Ti\text{-}Phl_{24}Fe\text{-}East_{19}Mus_2East_2Phl_{26}$. The compositions of Bt from quartz-diorites, granodiorites and granites are very similar. Biotite contains inclusions of Ap, Mt and Zrn. Plagioclase is present as phenocrysts, glomerules and as part of the matrix. It shows a distinctive oscillatory zoning core, with interspersed bands of An_{53} and An_{19}. K-feldspar forms anhedral grains with abundant inclusions of Qtz, Bt and Pl. Occasionally, Kfs grains form glomerules of assembled poikilitic grains. Most Qtz is present as anhedral grains, but it forms subhedral grains in some facies. Zircons are included in Qtz, Bt, Kfs and Pl.

5. Geochemical features

A set of 47 samples were collected and analyzed for major and trace elements. These are 21 diorites, 5 Qtz-diorites, 15 tonalite-granodiorites and 11 granites. The criteria for rock classification and nomenclature were exposed in a previous item. Representative analyses, including the selected samples for geochronologic study, are listed in Table 1 (a complete list is given in the Supplementary Material; Appendix A). The main geochemical features and their comparisons with similar rocks of the Patagonian batholith are exposed below.

5.1. Major elements

As mentioned above, the studied intrusive Mesozoic rocks of the Bariloche region show a complete range of silica from basic to intermediate and acid terms (49–75 wt% SiO_2). Of these, the silicic compositions represented by tonalites and granodiorites dominate in more than 90% of the outcropping rocks at the level of erosion of the plutons. In general terms, these are comparable to other plutonic associations of the Patagonian batholith, south of the Bariloche area, and also similar to calcic series from other Cordilleran batholiths of North America (Frost et al., 2001). A salient feature is the presence of a silica gap, which is null within the range 58–60 wt% SiO_2, separating the more mafic members, diorites, form the Qtz-diorites. In the Harker diagrams (Fig. 3) the association Qtz-diorite-tonalite/granodiorite-granite shows a continuous trend with good negative correlations for Al_2O_3, CaO, FeO and MgO. Alkalis show a more scattered distribution with a marked tendency to positive correlation. These relations are compatible with magmatic fractionation trends. Diorites, to the left of the silica gap, show a scattered distribution for most major elements, possibly related to local accumulations of Hbl and Mt in agreement with the observed textural features. Our data reproduce the main geochemical signatures reported for Cordilleran granitoids and mafic rocks of the Patagonian batholith (Hervé et al., 2007; Pankhurst et al., 1999).

Some diorites have high values of Al_2O_3 (up to 20 wt%). These are also rich in FeO and CaO (>8 wt% in both). The MgO content of

Please cite this article in press as: Castro, A., et al., Petrology and SHRIMP U–Pb zircon geochronology of Cordilleran granitoids of the Bariloche area, Argentina, Journal of South American Earth Sciences (2011), doi:10.1016/j.jsames.2011.03.011

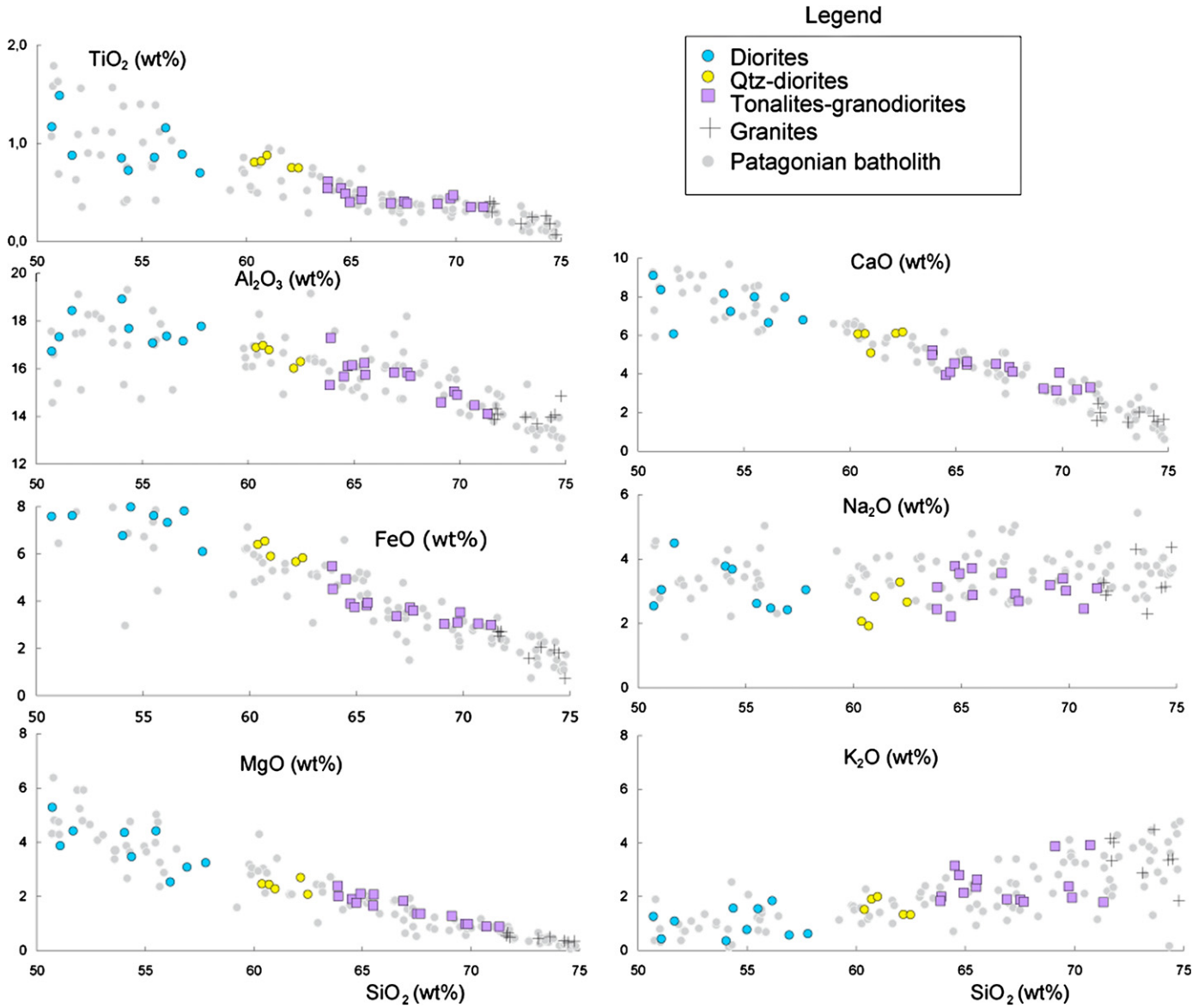

Fig. 4. Silica variation (Harker) diagrams plotting granitoids and mafic rocks of the Bariloche Cordilleran granitoids. Samples from the Patagonian batholith (Hervé et al., 2007; Pankhurst et al., 1999) are shown in the background.

this group is, however, very low (<5 wt% MgO). The high contents in Ca and Fe are correlated with the abundant Hbl and Mt in these rocks of possible cumulate origin. The low Mg content can be compatible with the cumulate origin if the fractionating magma is of intermediate composition. This will be discussed later. The scattered distribution of the more mafic rocks (diorites) also support the cumulate character controlled by mechanical processes that concentrate locally mafic minerals. By contrast, the linear patterns of the other group, approaching true *liquid lines of descent* is in support of processes of magma fractionation with the implication that intermediate and felsic rocks may have derived from nearly liquid systems.

The same inferences can be drafted based on the continuous curved trend displayed in the CaO–MgO diagram (Fig. 5a), a good proxy of cotectic relations in calc-alkaline magmas. A significant geochemical feature of these Cordilleran granitoids is the high Mg# (Mg# = molar MgO/MgO + FeO) for the intermediate terms of the series. Some tonalites and granodiorites may have values of up to Mg# = 0.5, contrasting with the more mafic Qtz-diorites that may have Mg# = 0.4 (Fig. 5b). The jump in Mg# is attributed to the onset of Mt precipitation in the system, which is correlated with the common presence of Mt in the more mafic rocks. This mineral may have played a significant role in magma fractionation.

5.2. Trace elements

A correlation of interest is found between Sr and Ca. These are coupled in magmatic fractionation, particularly in the granitic members of the series. The Sr content is correlated with the modal abundance of Pl. The maximum content is moderate (<600 ppm). Diorites are out of the Ca-Sr trend (Fig. 5c). They display an increase in Ca at constant Sr. This denotes the above-mentioned cumulate character of diorites, in which Cpx accumulation produces high Ca concentrations without partitioning of Sr. These coupled variations can be attributed to mineral assemblage, which in turn is pressure dependent. Model calculations will be shown

Please cite this article in press as: Castro, A., et al., Petrology and SHRIMP U–Pb zircon geochronology of Cordilleran granitoids of the Bariloche area, Argentina, Journal of South American Earth Sciences (2011), doi:10.1016/j.jsames.2011.03.011

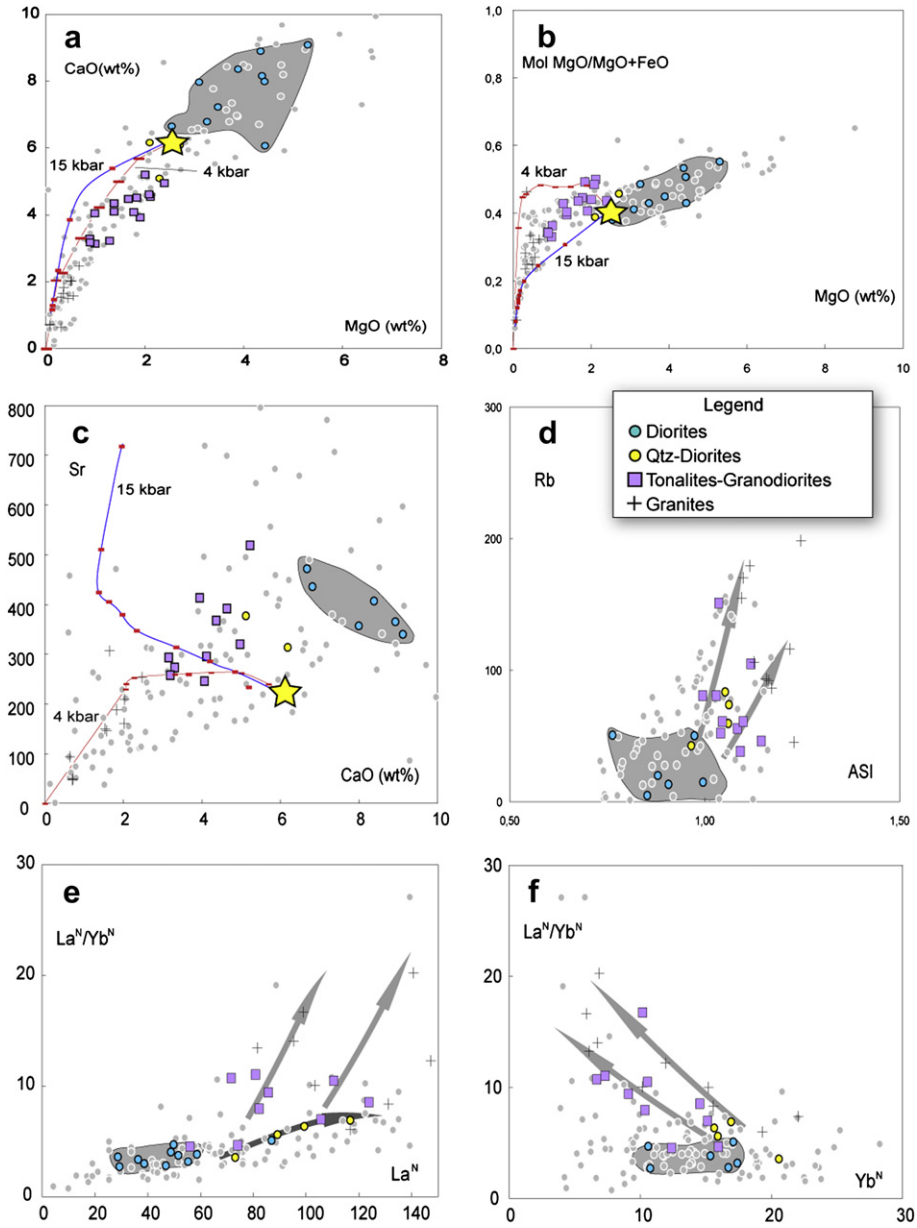

Fig. 5. Diagrams showing relevant geochemical variations of granitoids and mafic rocks of the Bariloche region. Major element (a, b) variations are compared with cotectic liquid compositions calculated with MELTS code for low (4 kbar, in red) and high (15 kbar, in blue) pressure and at fO_2 conditions of two log units greater than the QFM buffer. The parental liquid (large star) is a Qtz-diorite. Tick marks on the theoretical lines are 10 wt% liquid increments. In the CaO vs MgO diagram (a) the two cotectic lines are very close in composition and similar to the trend displayed by granodiorites-tonalites and granites. In the Mg# vs MgO diagram (b) the low-pressure line reproduces the jump in the Mg# denoting a larger effect of Mt fractionation at low-pressure. A drastic change from low to high pressure is depicted by the Sr–CaO diagram (c). The positive correlation between Rb and ASI (alumina saturation index) is denoting the implication of metaluminous phases (e.g. Hbl) in the fractionation process. Variations in the REE fractionation are shown in (e) and (f). Granitoid fractionation vectors (grey arrows) point to LREE enrichment together with HREE depletion in the more fractionated compositions. Note the parallel trends traced by granodiorites-tonalites and granites. (For interpretation of the references to colour in this figure legend, the reader is referred to the web version of this article.)

later for this coupled pair. The correlation found between the ASI and the Rb (Fig. 5d) is characteristic of fractionation processes dominated by metaluminous phases, namely Px and Hbl. The range of Sr/Y ratios of the studied rocks (Sr/Y = 2–40) are similar to other Cordilleran granites from Patagonia and North America. Although these values are lower than those of high-silica adakites (average Sr/Y = 60; Moyen, 2009), they are higher than most granites and the upper continental crust (2-20; Moyen, 2009 and references therein). Granites (SiO_2 > 71 wt%) display the lowest values of the Sr/Y ratio, ranging from 1 to 20. Granodiorites, Qtz-diorites and diorites are aligned along a parallel trend with higher values of the Sr/Y ratio.

Similar complex relations are displayed by REE (Fig. 6). All rocks are characterized by a little fractionation of the LREE with respect to HREE. Fractionation is more pronounced in the group of granodiorites and granites, which have La^N/Yb^N (N denoting chondrite-normalized values) ratios in the range 4–20 (average 10.5), compared with the lower values of 2–6 (average 4.6) of diorites and Qtz-diorites. Only the granite group (SiO_2 > 71 wt%) may show a negative Eu anomaly in some samples (Fig. 6), not necessarily the more silicic ones. This Eu anomaly is almost absent in the other groups of granitoids, namely tonalites, granodiorites and Qtz-diorites. Some samples of the diorite group may have an Eu positive anomaly, reinforcing the cumulate origin with the possible implication of Pl. The interpretation of these

Please cite this article in press as: Castro, A., et al., Petrology and SHRIMP U–Pb zircon geochronology of Cordilleran granitoids of the Bariloche area, Argentina, Journal of South American Earth Sciences (2011), doi:10.1016/j.jsames.2011.03.011

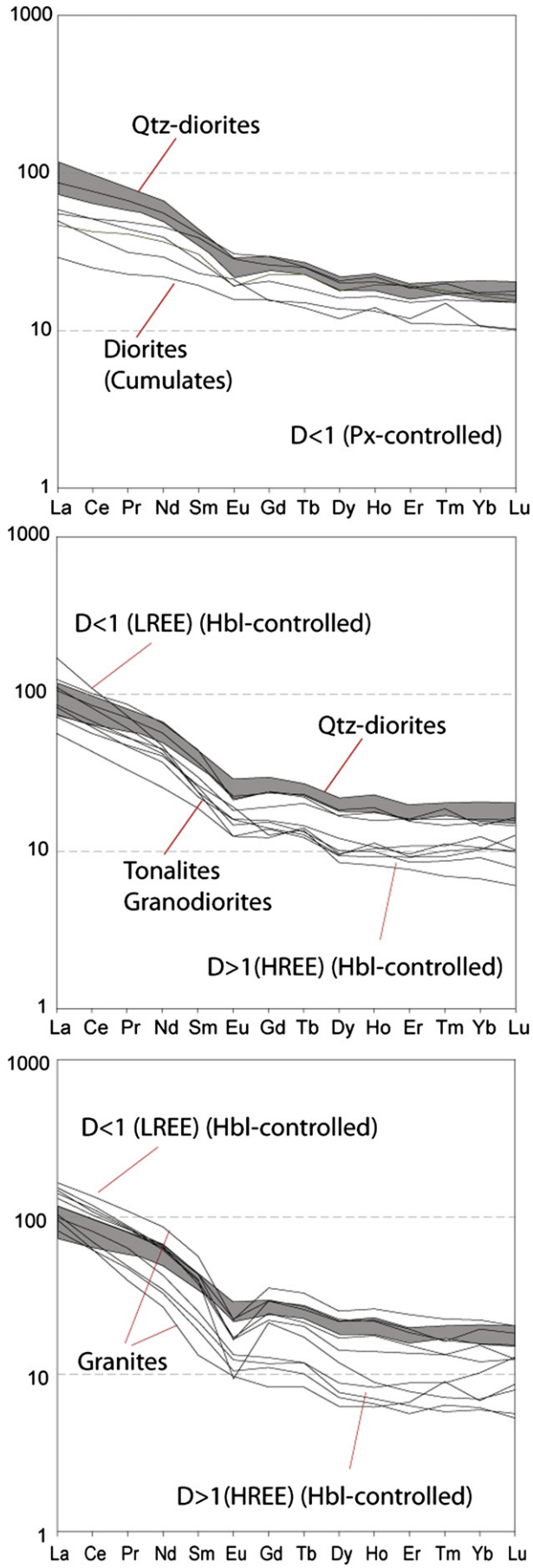

REE patterns in terms of magmatic fractionation will be given in a further section. The analyzed La^N/Yb^N ratios in the Bariloche region are similar to reported data from the Patagonian batholith (Hervé et al., 2007; Pankhurst et al., 1999). These are shown in Fig. 5e,f. Again, granites form a parallel trend pointing to more fractionated ratios coupled with both an increase in LREE and a decrease of the HREE. These trends are markedly different compared with the more regular variations of Qtz-diorites and the possible residual diorites. It can be highlighted that whereas the group of tonalites, granodiorites, Qtz-diorites and diorites plot within the ranges of typical Cordilleran batholiths in a Sr/Y vs La^N/Yb^N diagram (Fig. 7), the group of granites ($SiO_2 > 71$ wt%) plot outside this region with anomalously low Sr/Y ratios for moderate La^N/Yb^N values. Many of these geochemical ratios are strongly dependent on intensive variables, *P*, *T* and fO_2, which are conditioning the coexisting assemblage in the crystallizing magma and/or the melting process in the source region. Consequently, the determination of these intensive variables is fundamental to interpret the geochemical variations and decipher whether fractionation at the level of emplacement or melting at the source region was the dominant process involved in the formation of the rock association. An attempt to determine pressures and temperatures during magma emplacement is given here below. Further estimations will be shown later on basis to thermodynamic modeling.

6. Thermobarometry based on Hbl–Pl equilibria

Mineral chemistry data of amphibole–plagioclase pairs for diorites, quartz-diorites and tonalites were obtained for representative samples. Analytical results are given in the Supplementary Material (Appendix A). Amphibole and plagioclase are omnipresent, in different proportions but with similar textural and chemical features, as part of the mineral assemblage of diorites to granites of the batholith in the studied area. Amphiboles classify as Mg-hornblende [Si pfu = 6.55–7.26, $Mg/(Mg + Fe^{2+}) = 0.60–0.81$], tschermakitic hornblende [Si pfu = 6.48–6.44, $Mg/(Mg + Fe^{2+}) = 0.63–0.83$] and actinolitic hornblende [Si pfu = 7.28–7.50, $Mg/(Mg + Fe^{2+}) = 0.70–0.83$]. Barroisite and Mg-hastingsite [Si pfu = 6.18, $Mg/(Mg + Fe^{2+}) = 0.77$] have been analyzed from diorite chilled-margins. Most Amph is unzoned Mg-hornblende, but some grains show patchy zoning. They have low contents of TiO_2 which range from 2.25 wt% in diorites to 0.66 wt% in tonalites, most in the range between ca.1.3 to ca.0.7. Negative correlation of log Kd (TiO_2) with temperature suggests that these low TiO_2 contents mean low temperatures near the solidus of the diorite-tonalite system, in agreement with the presence of quartz in the same assemblage. Most Pl is present as phenocrysts and as part of the groundmass showing oscillatory-zoning. Al-in-hornblende barometer (Hammarstron and Zen, 1986; Schmidt, 1992), applied to single Hb-grains, shows that crystallization of Hb began at pressures lower than 6 kbar and followed to less than 1 kbar.

Sampled pairs of amphibole and plagioclase were analyzed in adjacent spots where Pl and Hb were apparently in textural equilibrium. *P–T* estimates for hornblende–plagioclase equilibrium were performed using an iterative method (Anderson, 1996) which combines Hb-Pl thermometry (Blundy and Holland, 1990; Holland and Blundy, 1994) with the Al-in-hornblende barometry (Schmidt, 1992; Anderson and Smith, 1995).

The closest range of pressure-temperature estimates after seven iterations are given for the calibration reaction edenite + albite = richterite + anorthite (Holland and Blundy, 1994) for temperature,

Fig. 6. Chondrite normalized (Nakamura, 1974) REE diagrams of representative intrusive rocks form the Bariloche region. The field of Qtz-diorites (grey) is taken as a reference in all diagrams.

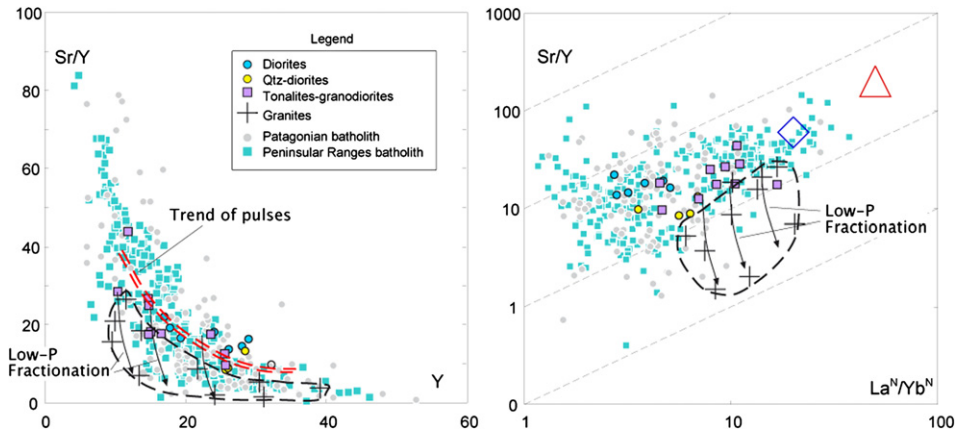

Fig. 7. Sr/Y vs Y (a) and Sr/Y vs La^N/Yb^N (b) diagrams plotting representative intrusive rocks from the Bariloche region. Diorites, Qtz-diortes and their fractionates (i.e.: granodiorites and tonalites) define a possible "trend of pulses" as supported by age-composition relations. Granites are plotted defining a parallel trend possibly related by fluid migration fractionation. Arrows mark the possible low-pressure (i.e. sub-volcanic) evolution from individual pulses of magma at late stages of fractionation. Samples from the Patagonian batholith (Hervé et al., 2007; Pankhurst et al., 1999) and from the Peninsular Ranges batholith in North America (Lee et al., 2007) are plotted in the background for comparisons.

combined with the calibration of Anderson and Smith (1995) of the Al-in-hornblende barometer. Anderson (1996) concluded that the calibration based on this reaction was the preferred calibration of the thermometer to work in conjunction with that Al-in-hornblende barometer. Most pressure estimates for diorites (ca. 2.5-1.2 kbar) are slightly higher than for quartz-diorites and tonalites (c.a. 2.0-0.7 kbar). For the last pressures, temperature estimates show similar relations, with slightly higher temperatures for diorites (ca. 826-747 °C) than for quartz-diorites and tonalites (ca. 792-650 °C). These *P–T* estimates correspond to near-solidus sub-volcanic conditions (s.l.) and are in agreement with cavities present in some of the studied zircon crystals, which were interpreted as a vapor phase trapped during crystallization of igneous zircons in a sub-volcanic environment (cf. Rapela et al., 2010).

7. Zircon geochronology

Representative samples of the most abundant and better-exposed intrusive bodies were selected for zircon separation and U–Pb geochronology via SHRIMP. A systematic sampling was carried out along transversal sections of intrusive bodies (e.g. Rio Manso section: 5 samples; Mascardi-Tronador section: 4 samples) with the aim of identifying age variations and compositional polarities orthogonal to the N–S structures. Other samples were collected from particular outcrops in which granites and mafic rocks show indications of coeval magmatic activity.

7.1. Sample descriptions and results

Most of the studied zircons show cavities piercing the cores, the rims, and even the grain boundaries. These cavities are interpreted as entrapments of a vapor phase in a sub-volcanic environment, reinforcing the low *P–T* estimations yielded by the Pl–Hb thermobarometry. No zircon inheritances were found. This, along with the observed zircon textures (e.g. euhedral shapes and core-rim zonations, see below), is an indication of a single igneous crystallization episode for zircons. Isotopic ratios and ages of the analyzed data points are listed in Table 3. Fig. 8 shows CL images and Concordia plot of two representative rocks, the Qtz-diorite A208-11 and the granite A208-33. Concordia plots from all studied rocks are shown in Fig. 9. A complete set of CL images is given in the Supplementary Material (Appendix A). A brief description of the studied samples and their analytical results are given here below.

7.1.1. A208-8

Rio Manso (41°30′30.1″, 71°47′30.9″). It is a Hbl-rich melanocratic rock (group D) showing mm scale banding in which fine-grained (<0.2 mm) layers composed of Pl and Mt alternate with Hbl-rich layers. Amphibole is a Mg-hornblende, anhedral and poikilitic with abundant inclusions of Mt. Relict inclusions of altered mafic minerals (Px?) are common. Pseudomorphosed Ol crystals showing the typical rhomboidal shape are commonly found. These are very similar in alteration products to the inclusions in Hbl. Apatite and zircon are accessory minerals.

Recovered zircon grains range in size from 106 μm to 276 μm. Zircon grains, both entire or fragments from the process of crushing, are subhedral to euhedral, mainly equant. CL images show that most grains consist of a core, which is sometimes embayed, surrounded by a banded overgrowth. Some grains are complex, consisting of a subhedral-unzoned core surrounded by three, banded and unzoned, overgrowths. Zircon cores are mainly unzoned, often bright. Zircon overgrowths show a variety of textures, banded and unzoned. U and Th contents are very high. U contents range from 276 to 4095 ppm, mostly greater than 1000 ppm U. High Th contents range from 182 to 14803 ppm, mostly greater than 1400 ppm. The Th/U ratios are >1 suggesting that zircons did not undergo a U loss event. The 7 analyzed grains, including cores and rims, yield concordant data. Five of the 7 analyzed areas form a single concordant group giving a Concordia age of 154 ± 1.8 Ma (MSWD = 1.7) that corresponds to Late Jurassic. There is not any evidence in the studied zircons of any old inherited zircon grain. Only one zircon age is off the main concordant group giving an age of 147.0 ± 2.0 Ma.

7.1.2. A208-29

Lago Mascardi – Tronador volcano (41°14′20.6″, 71°45′32.5″). This is a medium-grained, homogeneous, mesocratic to melanocratic rock (Group D), essentially composed of Hbl and Pl. Interstitial Qtz is common as a subordinate component. The rock is altered with abundant secondary minerals as Chl, Ep and Cc.

The zircons from this sample range in size from 75 μm to 116 μm. Some grains present skeletal cores surrounded by a banded overgrowth which ends with euhedral faces. A few grains show a sector-zoned core. Most grains consist of a dark or light subhedral-unzoned core surrounded by thin, banded overgrowths. The U content is moderate, ranging from 210 to 2070 ppm, mostly below 1000 ppm. Th contents are in the range between 262 and 3968 ppm, mostly under 1000 ppm. There are two zircon grains

Please cite this article in press as: Castro, A., et al., Petrology and SHRIMP U–Pb zircon geochronology of Cordilleran granitoids of the Bariloche area, Argentina, Journal of South American Earth Sciences (2011), doi:10.1016/j.jsames.2011.03.011

Table 3
SHRIMP isotopic ratios and ages of analyzed points in zircons from granitoids of the Bariloche region.

Grain spot	U ppm	Th ppm	Th/U	$^{206}Pb^*$ ppm	$^{206}Pb_c$ %	Isotopic ratios						Age (Ma)	
						$^{206}Pb^*/^{238}U$	Error ± %	$^{207}Pb^*/^{235}U$	Error ± %	$^{207}Pb^*/^{206}Pb^*$	Error ± %	$^{206}Pb/^{238}U$	$^{207}Pb/^{206}Pb$
SHRIMP zircon U–Pb data for sample A208-1													
2	69	116	1.75	1.46	0.00	0.02477	3.7	0.224	6.3	0.0657	5.1	157.7 ± 5.7	797 ± 110
3.1	871	869	1.03	19.7	0.29	0.02627	1.7	0.1750	2.9	0.0483	2.3	167.2 ± 2.8	114 ± 55
3.2	1731	190	0.11	37.5	0.03	0.02524	1.7	0.1742	2.1	0.05007	1.1	160.7 ± 2.7	198 ± 27
4	246	340	1.43	5.39	0.27	0.02542	1.8	0.1686	3.8	0.0481	3.3	161.8 ± 3.0	105 ± 78
5	690	270	0.4	15.5	0.09	0.02611	1.7	0.1768	2.7	0.04911	2.0	166.2 ± 2.9	153 ± 47
SHRIMP zircon U–Pb data for sample A208-6													
1	147	93	0.66	2.93	0.86	0.02310	2.2	0.154	8.4	0.0482	8.1	147.2 ± 3.2	111 ± 190
2	189	153	0.84	3.79	0.46	0.02325	2.1	0.1671	5.3	0.0521	4.9	148.2 ± 3.0	290 ± 110
3	182	151	0.86	3.70	0.58	0.02356	2.1	0.158	6.5	0.0487	6.1	150.1 ± 3.1	134 ± 140
4	145	74	0.53	3.14	0.60	0.02498	2.2	0.167	9.6	0.0485	9.4	159.1 ± 3.5	122 ± 220
5	129	84	0.67	2.68	0.00	0.02410	2.3	0.1744	5.6	0.0525	5.2	153.5 ± 3.5	307 ± 120
6	172	124	0.75	3.55	0.00	0.02404	2.2	0.180	5.6	0.0542	5.1	153.2 ± 3.3	381 ± 120
8	174	88	0.53	3.35	0.00	0.02245	2.2	0.165	7.8	0.0532	7.5	143.1 ± 3.1	336 ± 170
9	299	261	0.90	5.98	0.00	0.02331	2.0	0.1659	3.9	0.0516	3.3	148.5 ± 2.9	269 ± 77
10	176	132	0.77	3.58	0.98	0.02341	2.2	0.161	6.3	0.0500	5.9	149.2 ± 3.3	193 ± 140
11	128	134	1.09	2.66	0.42	0.02414	3.1	0.175	7.7	0.0527	7.1	153.8 ± 4.7	314 ± 160
12.1	1160	913	0.81	23.2	0.09	0.02324	1.8	0.1587	2.4	0.04951	1.7	148.1 ± 2.6	172 ± 39
12.2	139	76	0.56	3.08	6.82	0.02404	3.4	0.200	30	0.060	29	153.1 ± 5.2	614 ± 640
SHRIMP zircon U–Pb data for sample A208-8													
2	4095	3952	1.00	86.0	0.06	0.02443	1.7	0.1623	2.0	0.04818	1.0	155.6 ± 2.6	108 ± 24
3.1	4857	14803	3.15	96.3	0.05	0.02306	1.7	0.1550	1.9	0.04874	0.82	147.0 ± 2.5	135 ± 19
4	4108	5573	1.40	87.8	0.05	0.02486	1.8	0.1692	2.0	0.04938	0.91	158.3 ± 2.8	166 ± 21
5.2	1182	1770	1.55	25.0	0.25	0.02454	1.7	0.1643	2.7	0.04855	2.0	156.3 ± 2.7	126 ± 48
6.1	276	182	0.68	5.92	0.83	0.02475	2.7	0.170	9.2	0.0499	8.8	157.6 ± 4.2	188 ± 210
6.2	1390	1419	1.06	29.4	0.00	0.02466	1.7	0.1655	2.3	0.04869	1.5	157.0 ± 2.7	133 ± 35
7	2375	5010	2.18	49.3	0.16	0.02414	1.7	0.1628	2.2	0.04891	1.4	153.8 ± 2.6	143 ± 33
8.1	1365	1937	1.47	28.8	0.55	0.02444	1.7	0.1685	3.2	0.0500	2.7	155.6 ± 2.7	195 ± 62
8.2	879	1003	1.18	18.6	2.53	0.02398	1.9	0.246	7.9	0.0745	7.7	152.7 ± 2.8	1054 ± 150
SHRIMP zircon U–Pb data for sample A208-11													
1	55	48	0.91	1.25	2.15	0.02600	2.9	0.167	13	0.0466	12	165.5 ± 4.8	31 ± 290
2.2	87	75	0.89	2.06	1.43	0.02714	2.7	0.185	19	0.0494	19	172.6 ± 4.5	168 ± 450
3.1	81	40	0.51	1.73	0.66	0.02467	2.2	0.183	8.6	0.0539	8.3	157.1 ± 3.5	367 ± 190
4	115	109	0.98	2.59	2.18	0.02568	2.7	0.153	15	0.0432	15	163.5 ± 4.3	−155 ± 380
5.1	38	30	0.80	0.846	2.99	0.0250	4.2	0.158	37	0.046	37	159.1 ± 6.6	−8 ± 880
5.2	75	42	0.58	1.66	1.99	0.02532	2.4	0.169	15	0.0484	15	161.2 ± 3.8	117 ± 350
6.1	42	32	0.78	0.904	1.44	0.02473	2.8	0.202	15	0.0593	15	157.5 ± 4.4	577 ± 320
6.2	51	29	0.59	1.08	1.86	0.02422	2.8	0.164	22	0.049	22	154.3 ± 4.2	146 ± 520
8.1	86	84	1.01	1.91	0.75	0.02573	2.3	0.206	9.1	0.0582	8.8	163.8 ± 3.7	537 ± 190
8.2	96	49	0.53	2.14	0.50	0.02572	2.1	0.184	7.1	0.0519	6.8	163.7 ± 3.4	281 ± 160
SHRIMP zircon U–Pb data for sample A208-13													
1	290	198	0.70	6.74	0.55	0.02685	1.8	0.1790	3.9	0.0484	3.4	170.8 ± 3.1	117 ± 81
2	50	45	0.93	1.14	2.58	0.02585	2.5	0.191	14	0.0535	14	164.5 ± 4.0	349 ± 320
3	192	172	0.92	4.32	0.89	0.02593	2.0	0.168	9.7	0.0470	9.5	165.0 ± 3.2	48 ± 230
4.1	218	228	1.08	5.10	0.00	0.02726	1.9	0.2002	3.6	0.0533	3.1	173.4 ± 3.3	340 ± 69
4.2	299	280	0.97	7.14	1.15	0.02746	1.9	0.217	6.3	0.0572	6.0	174.6 ± 3.2	500 ± 130
5	189	203	1.11	4.17	0.50	0.02549	1.9	0.180	7.5	0.0513	7.2	162.3 ± 3.2	254 ± 170
6	182	165	0.93	4.20	0.37	0.02669	1.9	0.171	6.1	0.0466	5.8	169.8 ± 3.2	28 ± 140
7	22	13	0.63	0.546	3.82	0.02779	3.5	0.256	23	0.067	23	176.7 ± 6.1	833 ± 470
8	172	107	0.64	3.90	0.26	0.02634	1.9	0.1936	4.5	0.0533	4.1	167.6 ± 3.2	341 ± 93
SHRIMP zircon U–Pb data for sample A208-14													
1	101	111	1.14	2.37	3.14	0.02655	2.7	0.153	15	0.0418	15	168.9 ± 4.5	−240 ± 380
2.2	59	50	0.87	1.42	2.44	0.02743	3.0	0.204	29	0.054	29	174.4 ± 5.2	373 ± 650
2.1	92	113	1.27	2.18	2.31	0.02692	2.2	0.203	6.5	0.0547	6.1	171.2 ± 3.7	401 ± 140
SHRIMP zircon U–Pb data for sample A208-20													
1	63	69	1.12	1.46	1.78	0.02634	2.6	0.184	15	0.0508	15	167.6 ± 4.3	231 ± 350
2	118	93	0.81	2.75	1.69	0.02653	2.2	0.185	15	0.0507	15	168.8 ± 3.7	228 ± 350
3	133	108	0.84	3.10	1.16	0.02679	2.2	0.184	13	0.0498	13	170.4 ± 3.7	184 ± 310
5	173	147	0.88	4.18	1.14	0.02780	2.0	0.198	7.1	0.0516	6.8	176.8 ± 3.4	269 ± 160
6	235	241	1.06	5.36	0.00	0.02656	1.9	0.2003	3.6	0.0547	3.0	169.0 ± 3.2	400 ± 68
7	116	118	1.05	2.83	1.66	0.02804	2.1	0.193	9.6	0.0499	9.4	178.2 ± 3.7	193 ± 220
8	193	170	0.91	4.65	1.22	0.02778	2.1	0.169	14	0.0441	14	176.6 ± 3.6	−104 ± 350
10	119	95	0.83	2.69	1.44	0.02584	2.2	0.190	12	0.0533	11	164.5 ± 3.6	344 ± 260
SHRIMP zircon U–Pb data for sample A208-22													
1.1	359	925	2.66	7.90	0.61	0.02536	1.9	0.17	6.1	0.0499	5.8	161.4 ± 3.0	188 ± 136
2	120	139	1.19	2.80	1.22	0.02670	2.2	0.18	7.2	0.0491	6.9	169.9 ± 3.6	155 ± 161
4	238	277	1.20	5.50	0.35	0.02665	1.9	0.19	4.0	0.0517	3.6	169.6 ± 3.1	272 ± 82
5	222	95	0.45	5.10	0.63	0.02670	1.9	0.19	8.6	0.0506	8.4	169.8 ± 3.3	224 ± 193

(*continued on next page*)

Please cite this article in press as: Castro, A., et al., Petrology and SHRIMP U–Pb zircon geochronology of Cordilleran granitoids of the Bariloche area, Argentina, Journal of South American Earth Sciences (2011), doi:10.1016/j.jsames.2011.03.011

Table 3 (*continued*)

Grain spot	U ppm	Th ppm	Th/U	$^{206}Pb^*$ ppm	$^{206}Pb_c$ %	Isotopic ratios						Age (Ma)	
						$^{206}Pb^*/^{238}U$	Error ± %	$^{207}Pb^*/^{235}U$	Error ± %	$^{207}Pb^*/^{206}Pb^*$	Error ± %	$^{206}Pb/^{238}U$	$^{207}Pb/^{206}Pb$
6	244	277	1.17	5.50	0.66	0.02618	1.9	0.18	6.0	0.0508	5.7	166.6 ± 3.2	232 ± 132
7	144	116	0.83	3.20	0.37	0.02583	2.0	0.20	5.5	0.0559	5.1	164.4 ± 3.3	448 ± 113
9	246	306	1.29	5.70	0.71	0.02703	1.9	0.18	6.7	0.0489	6.4	172.0 ± 3.2	145 ± 151
10	310	527	1.76	7.10	0.89	0.02651	1.9	0.17	5.8	0.0470	5.5	168.7 ± 3.1	47 ± 131
11	38	33	0.90	0.90	3.09	0.02678	2.8	0.19	12.7	0.0522	12.4	170.3 ± 4.7	294 ± 283
SHRIMP zircon U–Pb data for sample A208-29													
1	391	684	1.81	9.41	5.54	0.02642	3.0	0.404	9.5	0.1109	9.0	168.1 ± 5.0	1814 ± 160
2	2070	3722	1.86	48.0	0.06	0.02696	2.7	0.1837	2.9	0.04940	1.2	171.5 ± 4.5	167 ± 28
3	886	914	1.07	20.4	0.08	0.02680	2.7	0.1804	3.1	0.04882	1.6	170.5 ± 4.5	139 ± 37
4	2021	3968	2.03	45.9	0.27	0.02634	2.7	0.1734	3.1	0.04775	1.6	167.6 ± 4.4	87 ± 37
5	210	245	1.20	4.81	1.45	0.02627	2.8	0.198	8.8	0.0547	8.3	167.1 ± 4.7	399 ± 190
7	676	1106	1.69	16.4	0.19	0.02813	2.7	0.1933	3.9	0.0498	2.8	178.8 ± 4.8	188 ± 65
9	652	262	0.42	15.5	0.25	0.02762	2.7	0.1948	3.5	0.0511	2.2	175.6 ± 4.7	247 ± 51
10	811	633	0.81	19.9	2.98	0.02765	2.8	0.212	12	0.0555	12	175.8 ± 4.9	434 ± 260
11	1630	1139	0.72	41.3	4.95	0.02807	2.8	0.204	10	0.0527	9.7	178.4 ± 4.8	314 ± 220
SHRIMP zircon U–Pb data for sample A208-31													
1	145	108	0.77	3.39	1.08	0.02692	2.8	0.162	6.2	0.0437	5.5	171.2 ± 4.8	−126 ± 140
2	257	280	1.12	6.11	1.30	0.02728	2.8	0.161	6.3	0.0428	5.6	173.5 ± 4.8	−182 ± 140
3	192	176	0.95	4.60	0.81	0.02764	2.9	0.185	9.9	0.0484	9.5	175.7 ± 5.0	121 ± 220
4	166	157	0.98	3.79	0.00	0.02662	2.9	0.1966	4.4	0.0536	3.3	169.4 ± 4.8	352 ± 74
5	71	62	0.89	1.72	1.52	0.02764	3.1	0.188	11	0.0494	11	175.8 ± 5.3	166 ± 260
6	255	258	1.05	6.12	0.46	0.02785	2.8	0.1967	5.1	0.0512	4.2	177.1 ± 4.9	252 ± 97
7	141	104	0.76	3.22	0.32	0.02647	3.3	0.197	5.8	0.0539	4.7	168.4 ± 5.5	368 ± 110
8	390	282	0.75	9.06	1.80	0.02652	2.8	0.197	9.6	0.0539	9.2	168.8 ± 4.7	368 ± 210
10	419	412	1.01	9.72	0.39	0.02687	2.8	0.1824	3.9	0.0492	2.7	171.0 ± 4.7	159 ± 64
11	229	165	0.74	5.02	0.32	0.02544	2.8	0.167	6.6	0.0476	6.0	162.0 ± 4.5	82 ± 140
12	79	49	0.64	2.07	10.66	0.0273	3.9	0.210	37	0.056	37	173.8 ± 6.7	444 ± 830
SHRIMP zircon U–Pb data for sample A208-33													
2	41	16	0.40	0.842	0.00	0.02377	3.4	0.194	8.2	0.0591	7.4	151.5 ± 5.2	569 ± 60
4.1	739	225	0.31	15.9	0.00	0.02502	2.8	0.1677	3.4	0.04861	2.0	159.3 ± 4.4	129 ± 46
4.2	489	179	0.38	10.3	0.29	0.02446	2.7	0.1612	3.9	0.0478	2.7	155.8 ± 4.2	90 ± 65
5	488	508	1.08	10.5	0.17	0.02501	2.7	0.1787	3.9	0.0518	2.8	159.3 ± 4.3	278 ± 63
6.1	926	229	0.26	20.0	0.08	0.02515	3.0	0.1709	3.6	0.0493	2.0	160.1 ± 4.7	162 ± 48
6.2	849	227	0.28	17.6	0.19	0.02411	2.7	0.1620	3.3	0.04874	1.8	153.5 ± 4.1	136 ± 43
7	322	81	0.26	6.92	0.25	0.02496	2.8	0.1710	4.9	0.0497	4.1	158.9 ± 4.4	180 ± 95
8	110	84	0.79	2.29	1.20	0.02401	3.0	0.168	11	0.0507	11	153.0 ± 4.6	226 ± 250
9	759	199	0.27	16.6	0.18	0.02545	2.7	0.1722	3.6	0.0491	2.3	162.0 ± 4.3	151 ± 55
10	199	310	1.61	4.15	0.25	0.02422	2.8	0.1605	5.1	0.0481	4.2	154.3 ± 4.3	102 ± 100
11	808	326	0.42	16.8	0.09	0.02419	2.7	0.1639	3.4	0.04914	2.0	154.1 ± 4.1	155 ± 47
12	737	686	0.96	15.9	0.18	0.02509	2.7	0.1699	3.4	0.04911	2.0	159.7 ± 4.3	153 ± 47
SHRIMP zircon U–Pb data for sample A208-48													
1	473	248	0.54	11.5	0.26	0.02812	2.7	0.1903	4.1	0.0491	3.0	178.8 ± 4.8	151 ± 71
2	392	225	0.59	9.52	0.22	0.02825	2.8	0.1966	4.6	0.0505	3.7	179.6 ± 4.9	218 ± 85
3	721	405	0.58	16.8	0.20	0.02714	2.7	0.1839	3.7	0.0491	2.5	172.6 ± 4.6	155 ± 58
4	670	334	0.51	15.9	0.23	0.02750	2.7	0.1809	3.7	0.0477	2.6	174.9 ± 4.7	85 ± 61
5	305	180	0.61	6.80	0.34	0.02586	3.0	0.1790	4.6	0.0502	3.5	164.6 ± 4.8	205 ± 82
6	767	451	0.61	17.9	0.00	0.02718	2.7	0.1864	3.2	0.04974	1.7	172.9 ± 4.6	183 ± 39
7	808	460	0.59	18.5	0.00	0.02663	2.7	0.1814	3.1	0.04940	1.6	169.4 ± 4.5	167 ± 36
8	417	272	0.67	9.63	0.47	0.02677	2.7	0.1861	3.9	0.0504	2.8	170.3 ± 4.6	215 ± 65
9	372	313	0.87	8.59	0.27	0.02678	2.8	0.1820	4.1	0.0493	3.0	170.4 ± 4.7	162 ± 70
10	456	426	0.97	10.7	0.11	0.02741	2.7	0.1849	3.6	0.0489	2.4	174.3 ± 4.7	145 ± 56
11	336	206	0.63	8.01	0.00	0.02771	2.8	0.1971	3.7	0.0516	2.4	176.2 ± 4.8	267 ± 55
12	624	779	1.29	14.8	0.11	0.02758	2.7	0.1920	3.3	0.05048	1.9	175.4 ± 4.7	217 ± 43

Errors are 1-sigma; Pb_c and Pb* indicate the common and radiogenic portions, respectively.
Error in Standard calibration was 0.73% (not included in above errors but required when comparing data from different mounts).
Common Pb corrected using measured ^{204}Pb.

with high contents of U and Th. Respectively, ca. 2050 ppm U and 3800 ppm Th. The Th/U ratios are mostly >0.2 as usual in zircons of magmatic origin (Hartmann et al., 2000). Eight of the 9 analyzed grains yield a concordant data giving a Concordia Age of 172.5 ± 3.1 Ma (MSWD = 0.97) that corresponds to the Middle Jurassic.

7.1.3. A208-14

Rio Manso (41°34′36.5″, 71°30′15.1″). This sample corresponds to a fine-grained, mesocratic rock (Group QD) essentially composed of Pl and Hbl with subordinate Qtz, Bt and Mt. Plagioclase is characteristically euhedral and shows a complex oscillatory zoning. Monomineralic Hbl aggregates (clots), 1–3 mm in diameter, are common. These normally have an external prismatic habit and are surrounded by Bt. Reaction from a precursor Px is the suggested interpretation for these mafic clots (Castro and Stephens, 1992). Quartz is typically poikilitic and Hbl may have both euhedral habit in crystals grown together with Qtz, and, more frequently, an anhedral habit surrounding Pl in Qtz-free areas.

Zircon grains of this sample are mostly equant, ranging in size from 75 μm to 116 μm. Most of them are euhedral or fragments of euhedral grains showing distinct zonation patterns. Usually, zircon grains present a clear unzoned core rimmed by oscillatory or sector-zoned overgrowths. Many grains show embayed grain boundaries. The U content is moderate to low, ranging from 59 to

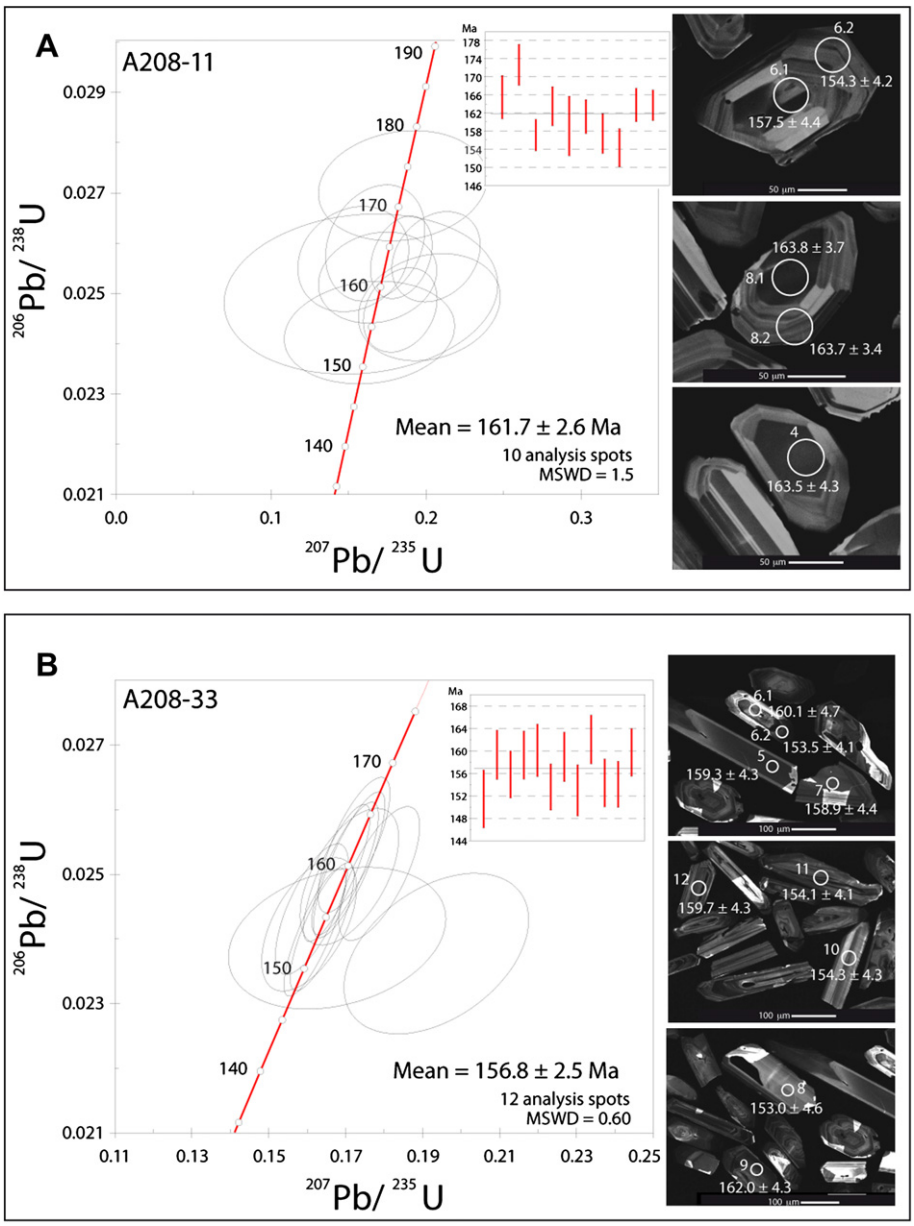

Fig. 8. Cathodoluminescence images and Concordia plots of two representative samples from the two main rock groups. A) A208-11 Qtz-diorite. B) A208-33 Granite.

101 ppm. Th contents range from 50 to 113 ppm. Th/U ratios are in the normal range for igneous zircon. The three analyzed grains yield a Concordia Age of 171 ± 5 Ma (MSWD = 0.33) corresponding to the Middle Jurassic.

7.1.4. A208-11

Rio Manso (41°35′42.2″, 71°45′41.5″). It is a coarse-grained, mesocratic rock (Group QD) essentially composed of Pl, Qtz and Hbl and subordinated Bt and Mt. Accessory minerals are Ap and Zrn. The rock has a hypidiomorphic texture, in which euhedral Pl is interlocked, and Qtz together with some Hbl occupy the interstices. Secondary minerals are Chl and Cc. Hornblende in these interstices is grown together with Qtz and is characterized by a euhedral habit. Other Hbl crystals form polycrystalline aggregates with an external prismatic shape, possibly formed by reaction from a precursor Px. Some of these clots are dominantly composed of Bt. Plagioclase shows a complex oscillatory zoning.

The zircons from this sample range from big, equant to elongate, entire or fragments of euhedral grains, ranging in size from 110.3 to 310.3 μm. The CL images show usually an unzoned core overgrown by rims showing mostly sector-zoning, or less frequently oscillatory zoning. Some zircons show jagged boundary grains interpreted as broken small cavities near the grain boundary. The U contents are relatively low, ranging from 38 to 115 ppm, most being less than 100 ppm. Th contents range from 29 to 109 ppm. Th/U ratios range from 0.51 to 1.01 being normal for igneous zircon. The ten analyzed spots yield a Concordia Age of 161.7 ± 2.6 Ma (MSWD = 1.5) corresponding to the Middle Jurassic.

7.1.5. A208-22

Lago Steffen (41°30′45.3″, 71°30′54.8″). It is an inequigranular leucocratic rock (Group TG) showing a porphyritic texture with phenocrysts of up to 5 mm in diameter of Pl and Qtz in a fine-grained felsitic matrix composed of Qtz, Pl and Kfs. Subordinate

Please cite this article in press as: Castro, A., et al., Petrology and SHRIMP U–Pb zircon geochronology of Cordilleran granitoids of the Bariloche area, Argentina, Journal of South American Earth Sciences (2011), doi:10.1016/j.jsames.2011.03.011

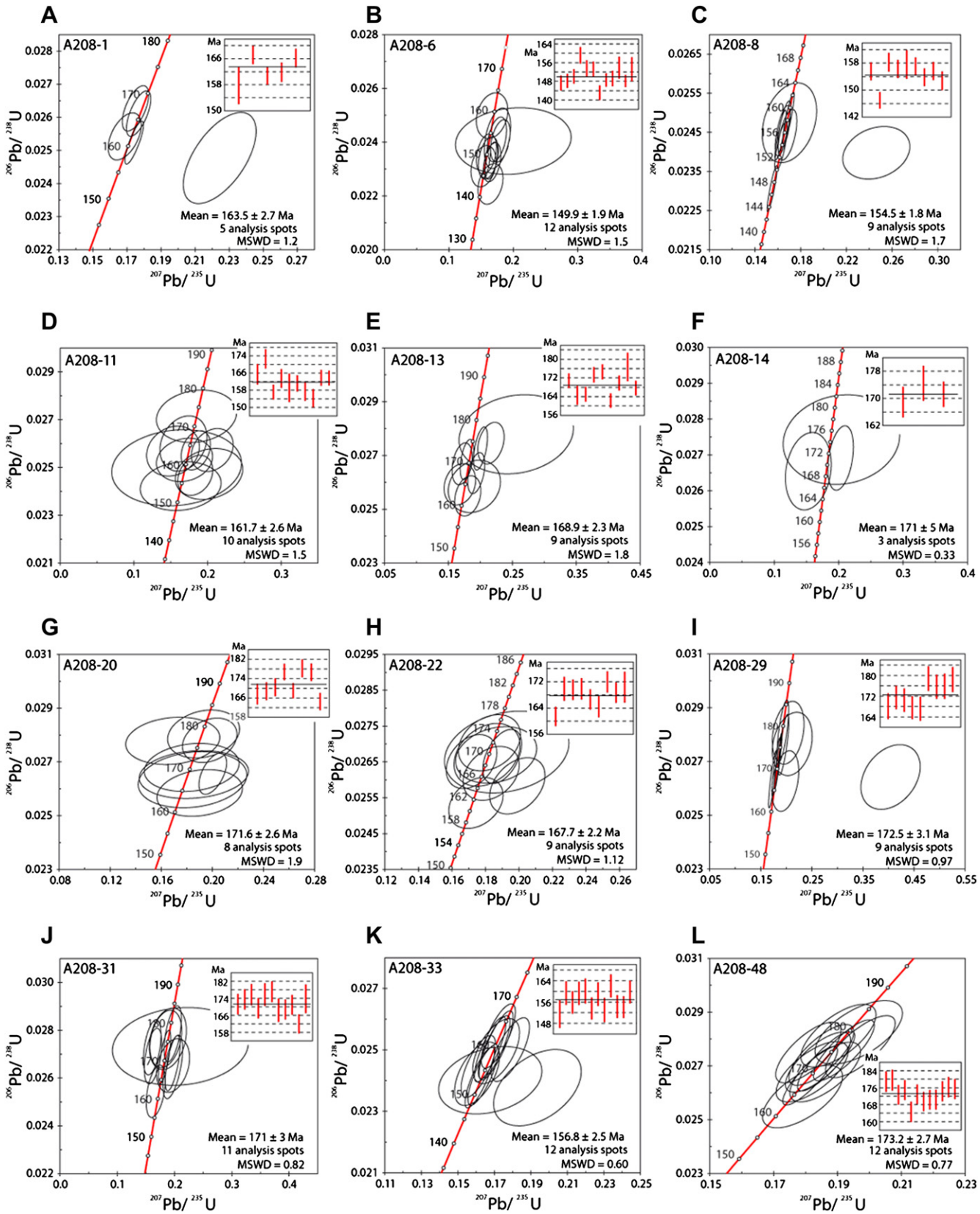

Fig. 9. Concordia plots of SHRIMP U–Pb isotopic analyses. Plots include 1σ error bars diagrams.

Please cite this article in press as: Castro, A., et al., Petrology and SHRIMP U–Pb zircon geochronology of Cordilleran granitoids of the Bariloche area, Argentina, Journal of South American Earth Sciences (2011), doi:10.1016/j.jsames.2011.03.011

minerals are Kfs, Hbl and Mt. Occasionally, Hbl forms polycrystalline aggregates that resemble phenocrysts of a precursor Px. Chlorite and Ep are common accessory minerals. Magnetite inclusions are frequently observed in Hbl aggregates.

Zircons from this sample range from relatively small, elongate, euhedral grains to big, elongate, euhedral grains, or fragments of these grains, ranging in size from ca. 76 μm to ca. 407 μm. CL images show typical igneous zircons consisting in a light or dark unzoned core rimmed with oscillatory zoning. Some grains present a longitudinal zonation that is consistent with an igneous origin. U contents are moderate to low, ranging from 38 to 359 pp. Th contents are correspondingly moderate, ranging from 33 to 925 ppm. Th/U ratios range from 0.42 to 2.03, mostly >1, typical of igneous zircons. There are no evidences of zircon inheritances. The nine analyzed spots yield a Concordia Age of 167.7 ± 2.2 Ma (MSWD = 1.12) that corresponds to the Middle Jurassic.

7.1.6. A208-6

Rio Manso (41°30′30.1″, 71°50′35.5″). It corresponds to a coarse-grained leucocratic rock (Group TG) composed of Pl and Qtz, with subordinate Bt and Kfs. Magnetite, apatite and zircon are common accessory minerals. The rock is altered with abundant secondary minerals such as Chl, Ep and sericite. Zircons from this sample range from equant to elongate, big euhedral grains, or fragments of these grains, ranging in size from 119.0 to 419.0 μm. CL images show either an anhedral unzoned core or an euhedral unzoned core, rimmed by oscillatory zoning. Some grains show a longitudinal pattern of zonation and some others show sector-zoning rims. The zonation patterns as shown by CL images are normal for igneous zircons. U contents are moderate, ranging from 128 to 1160 ppm, mostly larger than 150 ppm. Th contents are correspondingly moderate, ranging from 76 to 913 ppm. There is a good covariance between U and Th contents. Consistently, Th/U ratios range from 0.53 to 1.09 that is typical of igneous zircons. The twelve analyzed spots yield a Concordia Age of 149.0 ± 1.9 Ma (MSWD = 1.5) corresponding to the Late Jurassic.

7.1.7. A208-20

Lago Steffen (41°31′01.1″, 71°3209.1″). This is a coarse-grained leucocratic rock (Group G) composed of Kfs, Qtz and Pl with Hbl and Bt as subordinate minerals. Ap, Mt and Zrn are common accessory phases. Plagioclase crystals tend to be euhedral forming a framework with Kfs and Qtz occupying the interstices. Epidote, chlorite and sericite are common secondary minerals either replacing locally Bt or crystallized in veins and interstices between primary crystals. Quartz tends to form skeletal crystals giving to the rock a granophyric-like texture. Amphibole (Mg-Hbl) appears as tiny euhedral inclusions, together with Mt, in Kfs and Qtz, but never in Pl.

Zircons from this sample range from equant to elongate subhedral grains, or fragments of these grains, ranging in size from 78.8 to 272.7 μm. CL images show dark unzoned cores surrounded by differently developed oscillatory rims. Some grains show corroded cores, maybe related to cavities that are commonly found piercing the oscillatory rims and the cores. The U contents are low to moderate, ranging from 63 to 235 ppm. Th contents range from 60 to 241 ppm. Th/U ratios range from 0.45 to 2.66, normal values for igneous zircons. The analyzed spots do not yield a simple well-grouped cluster on the Wetherill plot but despite this, they provide a Concordia Age of 171.6 ± 2.6 Ma (MSWD = 1.9) that corresponds to the Middle Jurassic.

7.1.8. A208-13

Rio Manso (41°35′02.4″, 71°38′14.0″). It is a medium-grained leucocratic rock (Group G) composed of Pl, Kfs and Qtz and showing a typical hypidiomorphic texture. Euhedral Pl are enclosed by late, interstitial Qtz and Kfs. Subordinate minerals are Bt and Mt. Alteration products are Chl and Ep. Common accessory minerals are Hbl, Ap and Zrn. Bt and Hbl are included by Kfs and Qtz. Biotites are rich in Ap and Zrn inclusions.

The zircons from this sample are elongate, euhedral grains ranging in size from 50 to 303.6 μm. CL images show unzoned cores with oscillatory rims. Some grains show sector-zoning. U contents are low-moderate ranging from 22 to 290 ppm. Th contents show a good covariance with U, ranging from 13 to 280 ppm. The Th/U ratios (0.63–1.11) are in the normal range for igneous zircons. The nine analyzed spots yield a Concordia Age of 168.9 ± 2.3 Ma (MSWD = 1.8) that corresponds to the Middle Jurassic.

7.1.9. A208-31

Lago Mascardi- Tronador volcano (41°15′00″, 71°43′44.7″). It is a medium-grained, leucocratic and homogeneous rock (Group G) composed of Qtz, Pl and Kfs, showing a typical hypidiomorphic texture. Plagioclase tends to be euhedral and is weakly zoned. Quartz forms large polycrystalline aggregates with undulose extinction and subgrains. Subordinate Bt forms polycrystalline aggregates and is transformed to Chl. Zircon and Ap are common accessory phases.

The zircons from this sample range from equant to elongate, mostly euhedral or fragmented, with sizes ranging from 94.1 μm to 220.6 μm. CL images show a variety of igneous zonations mainly consisting in an euhedral to subhedral core rimmed by oscillatory zoning. Some grains show a longitudinal zoning interpreted as a section of the oscillatory rim. U contents are low-moderate ranging from 71 to 419 ppm most > 150 ppm. Th contents covariate with U, ranging from 49 to 412 ppm. Th/U ratios range from 0.64 to 1.12, which are normal for igneous zircons. The eleven analyzed spots yield a Concordia Age of 171 ± 3 Ma (MSWD = 0.82) that corresponds to the Middle Jurassic.

7.1.10. A208-33

Lago Mascardi – Tronador volcano (41°15′32.8″, 71°39′52.5″). This is a medium-grained leucocratic rock (Group G) composed of Qtz, Kfs and Pl and showing an allotriomorphic texture. Plagioclase tends to form euhedral and normally zoned crystals. Accessory minerals are Bt, Mt, Zm and Ap. Secondary Ms is common. Alteration products are Chl, Ep and sericite.

Zircons from this sample are big, clean, elongate, euhedral grains, ranging in size from 92.6 to 470.4 μm. CL images show typical igneous zircons with a clean, unzoned core rimmed by rims with oscillatory zoning. Some grains show longitudinal zoning. U contents are moderate to high, ranging from 41 to 926 ppm, although most of them show U contents larger than 400 ppm. Th contents range from 16 to 686 ppm. Th/U ratios present values between 0.26 and 1.61 that are in the normal range for igneous zircons, implying the absence of a Pb loss event. The analyzed spots formed a well-grouped cluster on the Wetherill plot that yield a Concordia Age of 156.8 ± 2.5 Ma (MSWD = 0.60) corresponding to the Late Jurassic.

7.1.11. A208-1

Lago Moreno (41°07′15.96″, 71°50′00.6″). This is a coarse-grained leucocratic and homogenous rock (Group G) composed of Qtz, Kfs and Pl and showing a typical hypidiomorphic texture. Plagioclase and Kfs tend to form large prismatic crystals (up to 10 mm). Tiny Pl inclusions are commonly found in Kfs. Subordinate Bt forms polycrystalline aggregates that occupy, together with Qtz, the interstices between feldspars. Secondary Ms and Chl are common. Quartz is a late crystallized phase and locally molds against plagioclase phenocrysts.

Please cite this article in press as: Castro, A., et al., Petrology and SHRIMP U–Pb zircon geochronology of Cordilleran granitoids of the Bariloche area, Argentina, Journal of South American Earth Sciences (2011), doi:10.1016/j.jsames.2011.03.011

Zircons from this sample are subhedral, elongate grains. Some are tabular. Grain size range from 74.2 to 312.9 μm. CL images show typical igneous zircons with unzoned cores rimmed by oscillatory zoning. Some cores are partially engulfed but rimmed by euhedral overgrowths. U contents are low to high, ranging from 69 to 1731 ppm. Th contents range from 116 to 869 ppm. Th/U ratios (0.11–1.75) are in the normal range for igneous zircons. The five analyzed spots yield a Concordia Age of 163.5 ± 2.7 Ma (MSWD = 1.2) corresponding to the Middle Jurassic.

7.1.12. A208-48

Villa Traful – Angostura (40°37′57.2″, 71°27′28.0″). This is a coarse-grained, porphyritic and leucocratic rock (Group G) very rich in Qtz and showing an allotriomorphic texture with Kfs. Albite-rich Pl and microcline form fine-grained aggregates and occasionally large (>4 mm) crystals, giving to the rocks a porphyritic appearance. Accessory phases are Bt, Hbl, Mt, Ap and Zrn. Zircons from this sample are elongate, euhedral grains, ranging in size from 111.5 to 365.4 μm. CL images show typical igneous zircons with light or dark unzoned cores rimmed by oscillatory zoning. U contents are moderate, ranging from 305 to 808 ppm. Th contents range from 206 to 779 ppm, showing a good covariance with U. Th/U ratios range from 0.51 to 1.29, most of them exceeding 0.6, being in the normal range for igneous zircons. The twelve analyzed spots form a well-grouped cluster on the Wetherill plot, yielding a Concordia Age of 173 ± 3 Ma (MSWD = 0.77) corresponding to the Middle Jurassic.

7.2. Summary of the geochronological results

Fig. 10 summarizes the geochronological results obtained in this work. Most of the dated granitoids (9 samples) are Middle Jurassic in age, and only three samples can be ascribed to Late Jurassic times. The age pattern keeps no particular relation with the composition of the granitoid (diorite, tonalite, granodiorite or granites can be indistinctly early or late). Also this study failed to find a clear spatial variation of granitoid ages in the studied area. The Cordilleran batholith appears clearly separated in time from the Early Jurassic magmatism represented by the Subcordilleran plutonic belt and the V1 volcanic event of the Chon Aike province (Pankhurst et al., 2000) (Fig. 10). On the other side, the Cordilleran granitoids are the correlative of the V2 volcanic event of Chon Aike (Pankhurst et al., 2000). Finally, the Late Jurassic granitoids are coeval to the Chon Aike V3 volcanic episode (Fig. 10).

8. Discussion

8.1. Magmatic fractionation: parental magma composition and depth

The observed geochemical variations in both major and trace elements, together with the textural and mineralogical relations, point to a roughly defined, overall process of magmatic "filtering" linking all the intrusive batholithic rocks of the Bariloche area. Cumulate diorites are possibly resulting from accumulation of Cpx (±Pl ± Mt) by escaping of a fluid-rich residual melt, and not by gravitational settling necessarily. This explains the absence of layered structures in the more mafic rocks (diorites), in which cumulate textures are observed. Cumulate Cpx was possibly transformed into Hbl clots that dominate the mineral assemblage of diorites. These contain abundant inclusions of Mt, indicating the important role of this mineral under high oxygen fugacity (fO_2) conditions. The most fractionated oxide by the action of the expelled fluid phase is silica, accounting for the pronounced silica gap between cumulate diorites and Qtz-diorites. This suggests that the composition of the parental magma that underwent fractionation may have a silica content within the range of the gap; i.e. an intermediate magma with SiO_2 = 58–60 wt%. Taking this reference composition, other oxides can be estimated at maximum values of MgO = 2.5 wt%, FeO = 6.5 wt%, CaO = 6.1. These are coincident with the typical compositions of evolved andesites (Green, 1982; Kelemen et al., 2003). Qtz-diorites represent the less fractionated liquids, and granites the most fractionated. However, the coexisting mineral assemblage at the time of fluid and/or fluid-rich melt extraction is changing with time due to the evolving conditions towards decreasing temperature and increasing silica content of the fractionating wet magma. Consequently, a drastic change is expected to occur from the early stages of fractionation, dominated by Cpx and Mt crystallization, to late stages at lower T and higher water content, dominated by Hbl + Pl fractionation and finally by Pl alone. These stages are inferred based on textural and mineralogical features. They have a decisive role in determining other trace-element signatures, particularly the REE. In the early stages, the REE behave as incompatible elements because they have solid/liquid partitioning coefficient (D) lower than unity for Cpx and Mt (Gill, 1981). Thus, they tend to be enriched in the residual liquid and not fractionated between them. The liquid at this stage is represented by the Qtz-diorites (Fig. 6a) with silica contents of about 60–62 wt%. From this stage onwards, in a system with decreasing T and increasing silica and fluids, the coexisting assemblage change to one

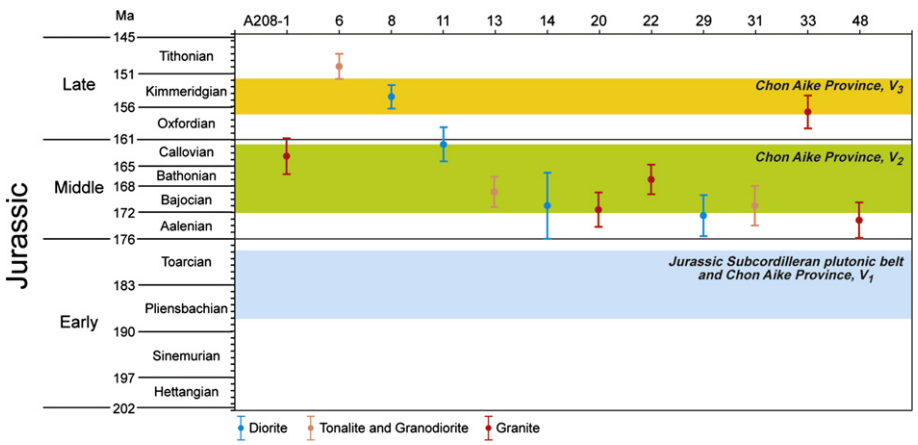

Fig. 10. Summary of the new zircon U–Pb SHRIMP radiometric dating of Cordilleran granitoids from the Bariloche region. Age ranges of the silicic volcanism in Patagonia (V1, V2 and V3 eruption events of Pankhurst et al., 2000) and the Subcordilleran plutonic belt (Rapela et al., 2005) are shown for comparison. Individual bars represent the age range from statistical analyses of the analyzed zircon populations.

Please cite this article in press as: Castro, A., et al., Petrology and SHRIMP U–Pb zircon geochronology of Cordilleran granitoids of the Bariloche area, Argentina, Journal of South American Earth Sciences (2011), doi:10.1016/j.jsames.2011.03.011

dominated by Hbl (±Pl). This implies an increase of D trespassing the threshold of compatibility ($D > 1$) for the HREE and preserving an incompatible behavior, $D < 1$ for the LREE (Rollinson, 1993 and references therein) in silica-rich system compositions. The implication is that REE will be depleted in the residual liquids and, at the same time, slightly fractionated. The abrupt change in the behavior of the REE with increasing silica is well appreciated in the REE patterns of granodiorites and tonalites (Fig. 6b). It is still more marked in the patterns of granites, some of which also record the presence of Pl in the coexisting mineral assemblage as denoted by the marked Eu negative anomaly (Fig. 6c). These relations are equally observed by comparing the normalized La^N/Yb^N ratios against the Yb^N and La^N contents (Fig. 5d,e). These show contrasted patterns for rocks with $SiO_2 < 60$ wt%, compared with the most silicic rocks ($SiO_2 > 62$ wt%).

According to Hbl thermobarometry, fractionation may have taken place, at least in part, at shallow pressures ($P = 0.7–2.5$ kbar), possibly at the level of emplacement. In spite of the consistency of these thermobarometric results in the different rock types of the series, it must be remarked that mineral compositions may have re-equilibrated to the final conditions during slow cooling. However, the shallow conditions of emplacement, and possibly of magma fractionation, are in agreement with the widespread observation of sub-volcanic textures, the habit of zircon crystals and the slightly or non metamorphosed country rocks, in many cases represented by eruptive deposits of the same age and composition than the intrusive rocks. All these data are indicating that most of the crystallization history of the magmas occurred at the shallow level of emplacement. We may conclude that Hbl was an important fractionating phase, and some evidences on this inference will be given below. However, part of the process of magma differentiation that produced the plutonic association started possibly at the source region and along its ascent through the continental crust until the shallow level of final emplacement. Mineral assemblages may be dependent on final conditions of crystallization, but changes in the melt compositions are initially controlled by the solid-melt phase equilibria at the source region at depth. The inference is that we may use rock compositions, properly identified as part of a *liquid line of descent* in magmatic systems undergoing fractionation, to compare with thermodynamic model calculations and constrain conditions at the source.

With these perspectives, fractionation has been modeled with MELTS code (Asimow and Ghiorso, 1998; Ghiorso and Sack, 1995) by assuming an initial liquid composition at the high-silica end of the compositional gap mentioned above. This is represented by the composition of Qtz-diorite. The model was run for several conditions by changing pressure and fO_2, for initial water content in the liquid of 2 wt% H_2O. Strong similarities between calculated *liquid lines of descent* and the rock trends were found for low-pressure (<4 kbar) and fO_2 buffered at QFM+2 for some geochemical parameters.

Models lines are plotted in some major–element diagrams (Fig. 5) that represent variations linked to multisaturation (e.g. cotectic) in a complex silicate magmatic system. In the CaO–MgO diagram (Fig. 5a), a proxy of cotectic evolution in calc-alkaline systems, the silicic groups represented by tonalites, granodiorites and granites fairly follow the calculated model. The less evolved terms may have equilibration temperatures of about 1000 °C. The *T* of about 800 °C measured by using the Hbl–Pl equilibria represent cooling temperatures at which the magma may have about 50 wt% liquid according to MELTS calculations. The same model calculations are used to obtain the variation of selected trace elements with fractionations. These are calculated by assuming equilibrium crystallization and a modal partitioning coefficient (Dm) calculated for the modeled phase assemblage at fixed increments of melts fractions (F).

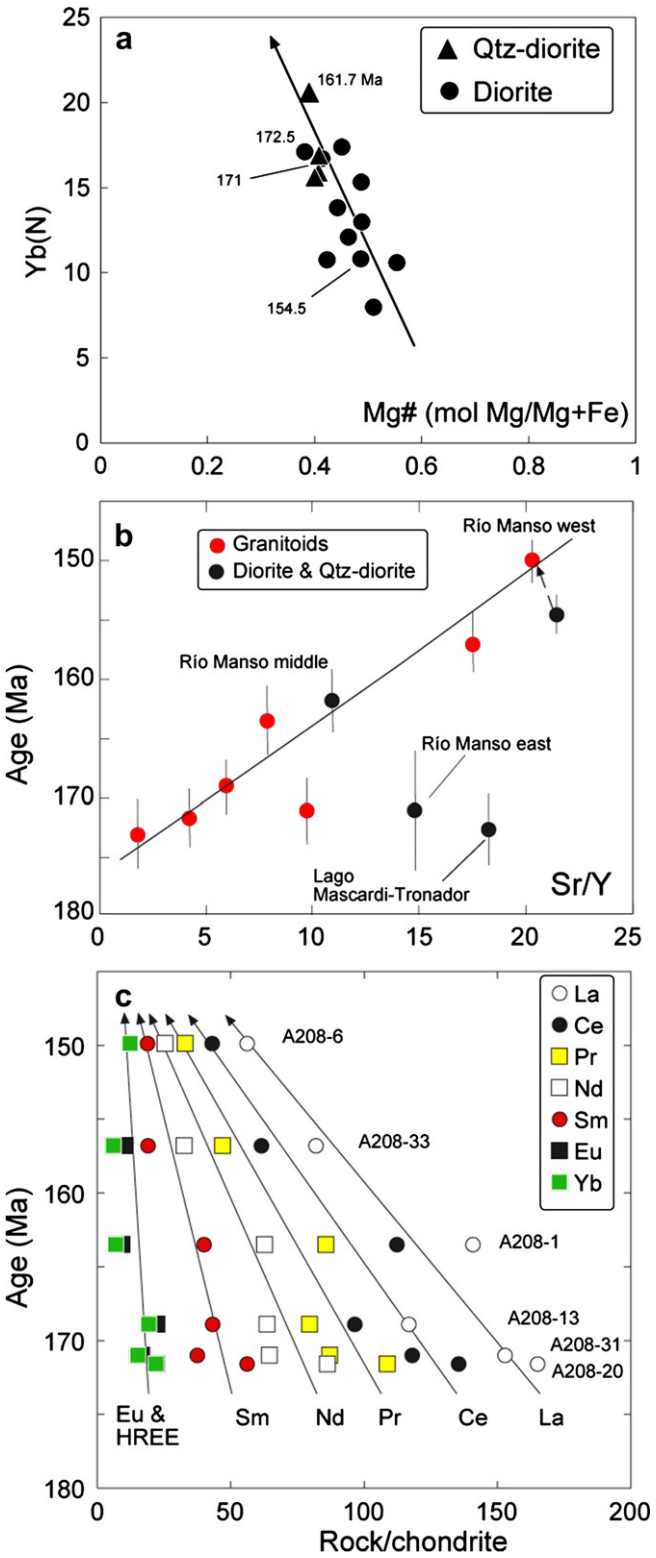

Fig. 11. Selected age-composition diagrams showing progressive changes in magma compositions with time. The correlation between Mg# and Yb in the mafic rocks (a) is denoting possible changes in the source region of magmas. The vector point to fractionation by reduction of the Mg# and increase in the abundance of incompatible elements (Yb). The vector is diachronic linking rocks separated by more than 15 Ma. Age and the Sr/Y ratio are positively correlated for granitoids (b) over a time interval of about 20 Ma. Data points represent discrete magma pulses and the increase in the Sr/Y ratio may record changing processes in the source region (e.g. pressure or composition). A decrease in LREE, but not in HREE, is correlated with decreasing age (c).

Please cite this article in press as: Castro, A., et al., Petrology and SHRIMP U–Pb zircon geochronology of Cordilleran granitoids of the Bariloche area, Argentina, Journal of South American Earth Sciences (2011), doi:10.1016/j.jsames.2011.03.011

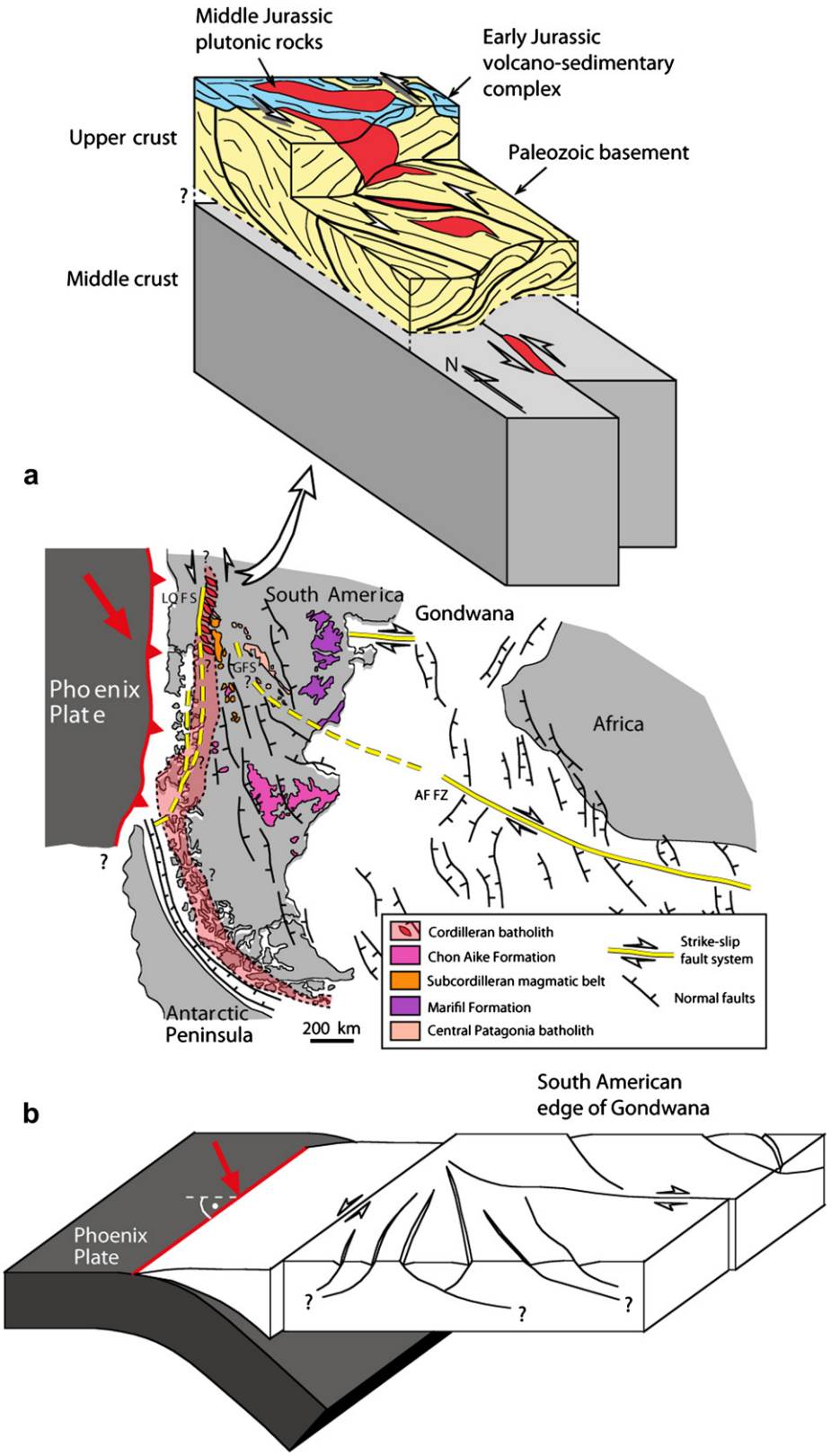

Fig. 12. Interpretative sketch of emplacement of the northern part of the Northern Patagonian batholith during the Middle Jurassic, according to the data presented in this work. (a) Middle Jurassic reconstruction of the South American margin of Gondwana. The large red arrow marks the supposed convergence vector for this time period (Zonenshayn et al., 1984; Mosquera and Ramos, 2006). LOFS: Liquiñe-Ofqui fault system. GFS: Gastre fault system. AFFZ: Agulhas-Falkland fracture zone. Modified from Uliana et al. (1989), Cembrano et al. (2000), Geuna et al. (2000), Hoffmann-Rothe et al. (2006), Mpodozis and Ramos (2008). The block diagram above the map illustrates the proposed mechanism of emplacement in the upper crust of the Cordilleran granitoids in the Bariloche area during the Middle Jurassic. (b) Schematic map and interpretative block diagram of the oblique subduction of the Phoenix plate under the South American margin of Gondwana during the Jurassic. (For interpretation of the references to colour in this figure legend, the reader is referred to the web version of this article.)

Please cite this article in press as: Castro, A., et al., Petrology and SHRIMP U–Pb zircon geochronology of Cordilleran granitoids of the Bariloche area, Argentina, Journal of South American Earth Sciences (2011), doi:10.1016/j.jsames.2011.03.011

The coupled Sr–Ca variation is shown in Fig. 5c with the same model parameters of the CaO–MgO diagram mentioned above. Data points and model can be compared qualitatively. The inflection in the slope at the limit between granites and granodiorites is related with the appearance of Pl in the system. This is fairly reproduced by the model. The dominant role of Pl in granites is also recorded by the pronounced negative Eu anomaly that characterizes this group.

The Sr/Y ratio is strongly dependent on the presence of Grt in the coexisting assemblage, and hence on pressure. This can be independent of the nature and composition of the source. However, these relations are not straightforward in water-undersaturated andesite systems (Green, 1982) due to two main reasons. First, the Grt stability boundary sharply changes with *T*, being almost independent on *T* for $T < 950$ °C, and strongly dependent on *T* at $T > 950$ °C. Second, Grt is not the liquidus phase for pressures below 23 kbar. The implication is that the diorite parental magma of the Bariloche granitoids may be located at relatively high pressure, at conditions close to the liquidus of the water-bearing andesite system (ca. 1100 °C) and without Grt in the source. Magmas extracted from this source in the lithsophere mantle may ascend adiabatically without crosscutting the Grt stability curve and, consequently, never undergoing REE fractionation or appreciable increase in the Sr/Y ratio. Coupled fractionation of Pl and Hbl at low-pressures may modify slightly the Sr/Y ratios of the parental magmas due to the compensating effect of these two phases for Sr that may yield a modal partitioning coefficient close to unity (Moyen, 2009).

The coupled observations of the two pressure dependent ratios, namely Sr/Y and La/Yb (Fig. 7) are pointing to a low-pressure, low-temperature final fractionation dominated only by Pl. This may account for the Sr/Y depletion in granitic rocks (SiO_2>71 wt%) that produce the parallel hyperbolic trend in the Sr/Y vs Y diagram (Fig. 7). This is compatible with the negative Eu anomaly of these granitic rocks denoting the role of Pl in the final fractionation process. The hyperbolic trend displayed by the parental Qtz-diorites and cumulates (diorites) may have been inherited from the source due to local changes in *P* and *T* conditions during melting and segregation. The implication of this interpretation is that the samples along the geochemical trend may correspond to individual magma pulses from the source, rather than regions of a big magma chamber. The relation between ages and compositions may help to solve this problem, of general applicability in other Cordilleran batholiths.

8.2. Time-composition relations: magma pulses from a deep-seated source?

One of the most important contributions from this study of Mesozoic granitoid rocks in the Bariloche region is the production of precise radiometric ages across magma bodies. The results of this study are crucial to understand the observed geochemical variations and the interpretation of magmatic processes. At a first-order approach, ages and compositions are independent. It is possible to identify early and late diorites as well as early and late granites and tonalites within a time interval of about 20 Ma. Although some compositional polarity can be identified within the group of granitic rocks, younger granites being relatively depleted in LREE and having the higher Sr/Y ratios (Fig. 11), an intriguing observation is that rocks forming a continuous geochemical trend are separated in age by about 10 Ma between then. This time interval is much longer than the maximum magma residence times of silicic shallow chamber (Halliday et al., 1989). The solution is that our fractionated magmatic rocks, which are aligned along geochemical trends that we interpret as *liquid lines of descent*, are in fact liquids intruded at different times in discrete pulses. The compositions of these magma pulses are constrained by solid-liquid phase equilibria at the source region and modified by magmatic fractionation at the level of emplacement at shallow levels. Which is in the geochemical patterns inherited form the source and which is created at the level of emplacement is not straightforward. This requires more detailed thermodynamic modeling and more precise age determinations. However, with these new data from radiometric dating and geochemical variations, it is possible to conclude that amalgamation of discrete magma pulses is the dominant process that built-up the batholith. Low-pressure geochemical fingerprints are dominant and obscure source-inherited features. For instance, the high Mg# displayed by the group of tonalites and granodiorites is interpreted by Mt fractionation at the level of emplacement considering a parental magma composition represented by the Qtz-diorites with SiO_2 ca. 60 wt% and MgO ca. 3 wt%. However, models with a dioritic source (not shown) fit better the fractionation of Mt at high pressure ($P > 10$ kbar). The meaning is that these systems are strongly controlled by high oxygen fugacity and Mt is a stable phase for wide pressure intervals from the source region to the emplacement level. Also interesting to note is the low Sr/Y ratios, similar to other Mesozoic Cordilleran batholiths along the America's active margin. These ratios are far from adakitic features in terms of pressure-temperature conditions, but a model based on partial melting of oceanic crust, cannot be ruled out. A potential silicic andesite protolith may have been produced at lithospheric pressures of about 15 kbar and at 1100–1200 °C in a region of the PT space out of the stability field of Grt. These conditions and source compositions have been tested by means of laboratory experiments and thermo-mechanical numerical modeling (Castro et al., 2010) giving melt compositions almost coincident in major and trace elements with the parental magmas of the Bariloche granitoids.

The silica content of this mafic precursor is critical in giving more or less silicic residual melts. Only mafic sources with a minimum silica content of 54 wt% are able to either fractionate to produce silicic melts with SiO_2>63 wt%. These sources are dioritic or andesitic and not basaltic. The addition of water may increase slightly the silica content in 1 wt% (Gaetani and Grove, 1998). Thus, the problem of the generation of silicic magmas is shifted back to the problem of primary andesite magma generation in the mantle wedge overlying the subducted lithosphere. The possible generation of silicic melts by melting of subducted mélanges, which intrude within the mantle wedge in the form of plumes, has been postulated (Castro et al., 2010). Batholiths can be a late consequence of these sublithospheric processes.

8.3. Batholith emplacement, age and relations with tectonic processes

The granitoids of the Cordilleran batholith at the Bariloche area were emplaced under low-pressure conditions, at shallow levels in the upper crust. A process of magmatic fractionation linked magma batches with contrasted compositions (from diorites to granites). The structural features of the granitoids and their host rocks (Figs. 1 and 2) are pointing to a double emplacement control. First, the size, tabular geometry and attitude of the pluton contacts and internal fabrics suggests the activity of a process of dike intrusion (Clemens and Mawer, 1992; Petford, 1996) in agreement with the mechanism proposed by Pankhurst et al. (1999) for the emplacement of the Northern Patagonian batholith in Chile. The orientation of the fractures that accommodated the granitoid intrusion is NW–SE to NNW–SSE, as shown by the structural data presented in this work (contacts and fabrics, Figs. 1 and 2). These fractures are oblique to the general N–S trend of the Patagonian batholith (inset in Fig. 1). Indeed, the map of the Bariloche region (Fig. 1) shows that the distinct plutonic bodies of the Cordilleran batholith are N–S aligned. The resulting geometry is compatible with the activity of

Please cite this article in press as: Castro, A., et al., Petrology and SHRIMP U–Pb zircon geochronology of Cordilleran granitoids of the Bariloche area, Argentina, Journal of South American Earth Sciences (2011), doi:10.1016/j.jsames.2011.03.011

a large-scale, sinistral, N–S trending, strike-slip fracture zone to which the local fractures permitting the emplacement of each magma pulse would be associated as secondary tensile or Riedel fractures (upper block diagram of Fig. 12). The magmatic and solid-state fabrics observed in the granitoids confirm this model. Therefore, it is suggested that the sinistral fault system described in this work, and responsible for the emplacement of the Cordilleran granitoids at Bariloche, could be considered as a major structure associated with the paleo-Liquiñe-Ofqui fault system. Pankhurst et al. (1992) highlighted the importance of the structural control of strike-slip faulting on the Andean magmatic episodes.

9. Conclusions

The North Patagonian batholith in Bariloche was accomplished by a protracted magmatic activity that lasted for about 20 Ma, between 150 and 170 Ma at the Medium Jurassic, according to U–Pb SHRIMP zircon determinations on 14 samples.

Geochemical and mineralogical data suggest that the composition of the parental magma that underwent fractionation may be an intermediate magma with SiO_2 = 58–60 wt%, MgO = 2.5 wt%, FeO = 6.5 wt%, CaO = 6.1. These are coincident with the typical compositions of evolved andesites. Magnetite, amphibole and plagioclase are the main phases involved in the fractionation process. According to Hbl thermobarometry, fractionation may have taken place, at least in part, at shallow pressures ($P = 0.5$–1.5 kbar), possibly at the level of emplacement.

It is concluded that amalgamation of discrete magma pulses is the dominant process that build-up the batholith. The resulting geometry of plutons is compatible with the activity of a large-scale, sinistral, N–S trending, strike-slip fracture zone permitting the emplacement of each magma pulse. This major, strike-slip fault system should be deeply entrenched in the crust to allow intruding magmas generated and fractionated at depth. Because batholith generation is a direct consequence of subduction, structural relations and ages can be used to constraint the plate motion relations during Jurassic in this region of the South America active margin.

Acknowledgments

The manuscript benefits with suggestions and criticisms by two anonymous referees. Sampling, petrology and SHRIMP studies were funded with research grants form the Spanish Ministry of Science and Innovation (Project CGL2007-63237/BTE). NM and GG received financial support from projects CGL2006-12415-CO3-01/BTE and CGL2009-13706-CO3-01. We thank the valuable help from Estanislao Godoy and Florencia Bechis during the first sampling campaign in Bariloche in 2008. AC thanks Xie Hangqiang for assistance with SHRIMP work in Beijing.

Appendix A. Supplementary material

Supplementary data associated with this article can be found in the online version. This material includes, (1) microphotographs, (2) microprobe data of minerals, (3) whole-rock geochemical compositions for major and trace elements and (4) CL images and Concordia plots of analyzed zircons.doi:10.1016/j.jsames.2011.03.011.

References

Anderson, J.L., 1996. Status of thermobarometry in granitic batholiths. Transactions-Royal Society of Edinburgh 87l, 125–138.

Anderson, J.L., Smith, D.R., 1995. The effects of temperature and fO_2 on the Al-in-hornblende barometer. American Mineralogist 80, 549–559.

Annen, C., Blundy, J.D., Sparks, R.S.J., 2006a. The genesis of intermediate and silicic magmas in deep crustal hot zones. Journal of Petrology 47, 505–539.

Annen, C., Scaillet, B., Sparks, R.S.J., 2006b. Thermal constraints on the emplacement rate of a large intrusive complex: the Manaslu Leucogranite, Nepal Himalaya. Journal of Petrology 47, 71–95.

Asimow, P.D., Ghiorso, M.S., 1998. Algorithmic modifications extending MELTS to calculate subsolidus phase relations. American Mineralogist 83, 1127–1132.

Blundy, J.D., Holland, T.J.B., 1990. Calcic amphibole equilibria and a new amphibole-plagioclase geothermometer. Contributions to Mineralogy and Petrology 104, 208–224.

Castro, A., Gerya, T.V., 2008. Magmatic implications of mantle wedge plumes: experimental study. Lithos 103, 138–148.

Castro, A., Gerya, T., García-Casco, A., Fernández, C., Díaz Alvarado, J., Moreno-Ventas, I., Loew, I., 2010. Melting relations of MORB-sediment mélanges in underplated mantle wedge plumes. Implications for the origin of Cordilleran-type batholiths. Journal of Petrology 51, 1267–11295.

Castro, A., Stephens, W.E., 1992. Amphibole-rich polycrystalline clots in calc-alkaline granitic rocks and their enclaves. Canadian Mineralogist 30, 1093–1112.

Cembrano, J., Schermer, E., Lavenu, A., Sanhueza, A., 2000. Contrasting nature of deformation along an intra-arc shear zone, the Liquiñe-Ofqui fault zone, southern Chilean Andes. Tectonophysics 319, 129–149.

Cingolani, C., Dalla Salda, L., Hervé, F., Munizaga, F., Pankhurst, R.J., Parada, M.A., Rapela, C.W., 1991. The magmatic avolution of northern Patagonia: new impresions of pre-Andean and Andean tectonics. In: Harmon, R.S., Rapela, C.W. (Eds.), Plutonismo from Antarctica to Alaska. Geological Society of America Special Paper 265, 29–44.

Clemens, J.D., Mawer, C.K., 1992. Granitic magma transport by fracture propagation. Tectonophysics 204, 339–360.

Collins, W.J., 2002. Hot orogens, tectonic switching, and creation of continental crust. Geology 30, 535–538.

Crawford, M.L., William, A., Crawford, W.M., Lindline, J., 2005. 105 million years of igneous activity, Wrangell, Alaska, to Prince Rupert, British Columbia. Canadian Journal of Earth Sciences 42, 1097–1116.

Cucchi, R.J., 1991. Las plutonitas de Pilahué, intrusivos jurásicos del sector occidental del macizo Norpatagónico. Revista de la Asociación Geológica Argentina 46, 181–187.

Currie, C.A., Beaumont, C., Huismans, R., 2007. The fate of subducted sediments: a case for backarc intrusion and underplating. Geology 35, 1111–1114.

DeCelles, P.G., Ducea, M., Kapp, P., Zandt, G., 2009. Cyclicity in Cordilleran orogenic systems. Nature Geoscience 2, 251–257.

Franchi, M.R., Page, R.F.N., 1980. Los basaltos cretácicos y la evolución magmática del Chubut occidental. Revista de la Asociación Geológica Argentina 35 (5), 208–229.

Frost, B.R., Barnes, C.G., Collins, W.J., Arculus, R.J., Ellis, D.J., Frost, C.D., 2001. A geochemical classification for granitic rocks. Journal of Petrology 42, 2033–2048.

Gaetani, G.A., Grove, T.L., 1998. The influence of water on melting of mantle peridotite. Contributions to Mineralogy and Petrology 131, 323–346.

García-Moreno, O., Castro, A., Corretgé, L.G., El-Hmidi, H., 2006. Dissolution of tonalitic enclaves in ascending hydrous granitic magmas: an experimental study. Lithos 89, 245–258.

García-Sansegundo, J., Farias, P., Gallastegui, G., Giacosa, R.E., Heredia, N., 2009. Structure of the Gondwanan basement in the Bariloche region (North Patagonian Argentine Andes). International Journal of Earth Sciences 98, 1599–1608.

Gerya, T.V., Yuen, D.A., Sevre, E.O.D., 2004. Dynamical causes for incipient magma chambers above slabs. Geology 32, 89–92.

Geuna, S.E., Somoza, R., Vizán, H., Figari, E.G., Rinaldi, C.A., 2000. Paleomagnetism of Jurassic and Cretaceous rocks in central Patagonia: a key to constrain the timing of rotations during the breakup of southwestern Gondwana? Earth and Planetary Science Letters 181, 145–160.

Ghiorso, M.S., Sack, R.O., 1995. Chemical mass transfer in magmatic processes. IV. A revised and internally consistent thermodynamic model for the interpolation and extrapolation of liquid–solid equilibria in magmatic systems at elevated temperatures and pressures. Contributions to Mineralogy and Petrology 119, 197–212.

Giacosa, R.E., Heredia, N., 2001. Hoja del Mapa Geológico de la República Argentina a Escala 1:250.000 n° 4172-IV (San Carlos de Bariloche). SEGEMAR-IGRM. Buenos Aires. Argentina, pp. 1–77.

Giacosa, R.E., Heredia, N., 2004. Structure of the north Patagonian thick-skinned fold and thrust belt, southern central Andes, Argentina (41°–42° S). Journal of South American Earth Sciences 18 (1), 61–72.

Giacosa, R., Afonso, J., Heredia, N., Paredes, J., 2005. Tectonics of Preandean sector of the north Patagonian Andes, southern central Andes of Argentina (41°–42° 30' S). Journal of South American Earth Sciences 20, 157–170.

Gill, J., 1981. Orogenic Andesites and Plate Tectonics. Springer-Verlag, Berlin. 380.

González Díaz, E.F., 1982. Chronological zonation of granitic plutonism in the northern Patagonian Andes of Argentina: the migration of intrusive cycles. Earth Science Reviews 18, 365–393.

González Díaz, E.F., Lizuaín, A., Ramos, V. (Eds.), 1984. Geología y Recursos Naturales de la Provincia de Río Negro. El Complejo volcano-clástico y plutónico del sector cordillerano 1 (13), 119–138.

González, E.F., Valvano, J., 1979. Plutonitas cretácicas y neoterciarias entre el sector norte del lago Nahuel Huapí y el lago Traful (Provincia del Neuquén). 7° Congreso Geológico Argentino, Actas 1, pp. 227–242. Buenos Aires.

Gordon, A., Ort, M., 1993. Edad y correlación del plutonismo subcordillerano en las provincias de Río Negro y Chubut. 12° Congreso Geológico Argentino, Buenos Aires, Actas 4, pp. 120–127.

Green, T.H., 1982. Anatexis of mafic crust and high pressure crystallization of andesite. In: Thorpe, R.S. (Ed.), Andesites: Orogenic Andesites and Related Rocks. John Wiley and Sons, Chichester, pp. 465–487.

Haller, M.J., Linares, M., Ostera, H.A., Page, S.M., 1999. Petrology and geochronology of the Subcordilleran Plutonic Belt of Patagonia, Argentina. II South American Symposium on Isotope Geology. Actas SEGEMAR, Buenos Aires, Carlos Paz, Argentina, pp. 210–214.

Hammarstron, J.M., Zen, E-An, 1986. Aluminium in hornblende: an empirical igneous geobarometer. American Mineralogist 71 (11–12), 1297–1313.

Hartmann, L.A., Leite, J.A.D., da Silva, L.C., Remus, M.V.D., McNaughton, N.J., Groves, D.I., Fletcher, I.R., Santos, J.O.S., Vasconcellos, M.A.Z., 2000. Advances in SHRIMP geochronology and their impact on understanding the tectonic and metallogenic evolution of southern Brazil. Australian Journal of Earth Sciences 47, 829–844.

Hawkesworth, C.J., Kemp, A.I.S., 2006. Evolution of the continental crust. Nature 443, 811–817.

Hervé, F., Pankhurst, R.J., Fanning, C.M., Calderon, M., Yaxley, G.M., 2007. The South Patagonian batholith: 150 my of granite magmatism on a plate margin. Lithos 97, 373–394.

Hoffmann-Rothe, A., Kukowski, N., Dresen, G., Echtler, H., Oncken, O., Klotz, J., Scheuber, E., Kellner, A., 2006. Oblique convergence along the Chilean margin: partitioning, margin-parallel faulting and force interaction at the plate interface. In: Oncken, O., Chong, G., Franz, G., Giese, P., Götze, H.J., Ramos, V.A., Strecker, M.R., Wigger, P. (Eds.), The Andes: Active Subduction Orogeny. Springer, Berlin, pp. 125–146.

Holland, T.J.B., Blundy, J., 1994. Non-ideal interactions in calcic amphiboles and their bearing on amphibole-plagioclase thermometry. Contributions to Mineralogy and Petrology 116, 433–447.

Kelemen, P.B., Hanghoj, K., Greene, A.R., 2003. One view of the geochemistry of subduction-related magmatic arcs, with emphasis on primitive andesite and lower crust. In: Rudnick, R.L. (Ed.), The Crust. Elsevier, Amsterdam, pp. 593–659.

Kemp, A.I.S., Hawkesworth, C.J., 2003. Granitic perspectives on the generation and evolution of the continental crust. In: Rudnick, R.L. (Ed.), Treatise on Geochemistry. The Crust, vol. 3. Elsevier-Pergamon, Oxford, pp. 349–410.

Kretz, 1983. Symbols for rock-forming minerals. American Mineralogist 68, 277–279.

Lackey, J.S., Valley, J.W., Saleeby, J.B., 2005. Supracrustal input to magmas in the deep crust of Sierra Nevada batholith: evidence from high-[delta]18O zircon. Earth and Planetary Science Letters 235, 315–330.

Le Bas, M.J., Le Maitre, R.W., Streckeisen, A., Zanettin, B., 1986. A chemical classification of volcanic rocks based on the total alkali-silica diagram. Journal of Petrology 27, 745–750.

Leake, B.E., Woolley, A.R., Arps, C.E.S., Birch, W.D., Gilbert, M.C., Grice, J.D., Hawthorne, F.C., Kato, A., Kisch, H.J., Krivovichev, V.G., Linthout, K., Laird, J., Mandarino, J., Maresch, W.V., Nickel, E.H., Rock, N.M.S., Schumacher, J.C., Smith, D.C., Stephenson, N.C.N., Ungaretti, L., Whittaker, E.J.W., Youzhi, G., 1997. Nomenclature of Amphiboles: report of the subcommittee on Amphiboles of the International Mineralogical Association Commission on new minerals and mineral names. Mineralogical Magacine 61, 295–321.

Lee, C.-T.A., Morton, D.M., Kistler, R.W., Baird, A.K., 2007. Petrology and tectonics of Phanerozoic continent formation: from island arcs to accretion and continental arc magmatism. Earth and Planetary Science Letters 263, 370–387.

Lizuaín, A., 1980. Las Formaciones Suprapaleozoicas y Jur·sicas de la Cordillera PatagÛnica. Provincias de RÌo Negro y Chubut. Revista de la AsociaciÛn GeolÛgica Argentina 25 (2), 174–182.

Lizuaín, A., 1981. Características y edad del plutonismo en los alrededores del lago Puelo-Provincia del Chubut. 8° Congreso Geológico Argentino, Actas 3, 607–616 (San Luis).

Lizuaín, A., 1983. Geología de la Cordillera Patagónica entre las localidades de Lago Puelo y Leleque. PhD Thesis, Universidad de Buenos Aires.

Ludwig, K.R., 2003. Mathematical-statistical treatment of data and errors for Th-230/U geochronology. Uranium-Series Geochemistry. Rewiews in Mineralogy and Geochemistry 52, 631–656.

Mosquera, A., Ramos, V.A., 2006. Intraplate deformation in the Neuquén Embayment. Special Paper. In: Kay, S.M., Ramos, V.A. (Eds.), Evolution of an Andean Margin: A Tectonic and Magmatic View from the Andes to the Neuquén Basin (35°–39°S lat), 407. Geological Society of America, pp. 97–123.

Moyen, J.F., 2009. High Sr/Y and La/Yb ratios: the meaning of the "adakitic signature". Lithos 112, 556–574.

Mpodozis, C., Ramos, V., 2008. Tectónica jurásica en Argentina y Chile: Extensión, subducción oblicua, rifting, deriva y colisiones? Revista de la AsociaciÛn GeolÛgica Argentina 63 (4), 481–497.

Nakamura, N., 1974. Determination of REE, Ba, Fe, Mg, Na and K in carbonaceous and ordinary chondrites. Geochimica et Cosmochimica Acta 38 (5), 757–775.

Pankhurst, R.J., Hervé, F., Rojas, L., Cembrano, J., 1992. Magmatism and tectonics in continental Chiloé, Chile. Tectonophysics 205, 283–294.

Pankhurst, R.J., Weaver, S.D., Hervé, F., Larrondo, P., 1999. Mesozoic-Cenozoic Evolution of the North Patagonian Batholith in Aysén, Southern Chile, 156. Journal of the Geological Society, London. 673–694.

Pankhurst, R.J., Riley, T.R., Fanning, C.M., Kelley, S.P., 2000. Episodic silicic volcanism in Patagonia and the Antarctic Peninsula: chronology of magmatism associated with the break-up of Gondwana. Journal of Petrology 41, 605–625.

Parada, M.A., Nyström, J.O., Levi, B., 1999. Multiple sources for the Coastal Batholith of central Chile 31–348S/: geochemical and Sr–Nd isotopic evidence and tectonic implications. Lithos 46, 504–521.

Passchier, C.W., Trouw, R.A.J., 1996. Microtectonics. Springer, Berlin Heidelberg New York, 1–304.

Petford, N., 1996. Dykes or diapirs? Transactions of the Royal Society of Edinburgh. Earth Sciences 87, 105–114.

Ramos, V.A., 1999. Rasgos estructurales del Territorio Argentino. In: Caminos, R. (Ed.), Geología de Argentina. Anales SEGEMAR, 29(24), pp. 715–784.

Ramos, V.A., Niemeyer, H., Skarmeta, J., Muñoz, J., 1982. Magmatic evolution of the Austral Patagonian Andes. Earth-Science Reviews 18, 411–443.

Rapela, C.W., 1999. El plutonismo Triásico-Jurásico de la Patagonia. In: Caminos, R. (Ed.), Geología Argentina. Anales. Instituto de Geología y recursos Minerales, Buenos Aires 29 (6), 364–372.

Rapela, C.W., Alonso, G., 1991. Litología y geoquímica del Batolito de la Patagonia Central. 6o Congreso Geológico Chileno, Actas 1, pp. 236–240.

Rapela, C.W., Pankhurst, R.J., Harrison, S.M., 1992. Triassic "Gondwana" granites of the Gastre district, north Patagonian massif. Transactions of the Royal Society of Edinburgh. Earth Sciences 83, 291–304.

Rapela, C.W., Pankhurst, R.J., Fanning, C.M., Hervé, F., 2005. Pacific subduction coeval with the Karoo mantle plume: the early Jurassic Subcordilleran belt of northwestern Patagonia. Special Publications. In: Vaughan, A.P.M., Leat, P.T., Pankhurst, R.J. (Eds.), Terrane Processes at the Margins of Gondwana, 246. Geologycal Society, London, pp. 217–239.

Rapela, C.W., Munizaga, L., Dalla Salda, L., Hervé, F., Parada, M., Cingolani, C., 1987. Nuevas edades K-Ar de los granitoides del sector nororiental de los Andes Patagónicos. 10° Congreso Geológico Argentino. Actas 4, 18–20. Tucumán.

Rapela, C.W., Pankhurst, R.J., Casquet, C., Baldo, E.G., Galindo, C., Fanning, C.M., Dahlquist, J.M., 2010. The Western Sierras Pampeanas: protracted Grenville-age history (1330-1030 Ma) of intra-oceanic arcs, subduction-accretion at continental-edge and AMCG intraplate magmatism. Journal of South American Earth Sciences 29, 105–127.

Rollinson, H., 1993. Using Geochemical Data. Longman, New York. 352 p.

Schmidt, M.W., 1992. Amphibole composition in tonalite as a function of pressure: an experimental calibration of the Al-in-horblende-barometer. Contributions to Mineralogy and Petrology 110, 304–310.

Silver, L.T., Chappell, B.W., 1988. The Peninsular ranges batholith: an insight into the evolution of the Cordilleran batholiths of southwestern north America. Transactions of the Royal Society of Edimburgh. Earth Sciences 79, 105–121.

Spikermann, J.P., Strelin, J., Marshall, P., Carrillo, R., Montenegro, T., Lago, M., Villalba, E., Pérez, A., 1988. Geología del área El Batolito de Aleusco, Departamento de Languiñeo, provincia de Chubut. Revista de la Asociación Argentina de Mineralogía, Petrología y Sedimentología 19 (1/4), 39–48.

Toubes, R., Spikermann, J., 1973. Algunas edades K/Ar y Rb/Sr de las plutonitas de la Cordillera Patagónica entre los paralelos 40-44 de latitud sur. Revista de la Asociación Geológica Argentina 28 (4), 382–396.

Uliana, M.A., Biddle, K.T., Cerdan, J., 1989. Mesozoic extension and the formation of Argentine sedimentary basins. In: Tankard, A., Balkwill, H.R. (Eds.), Extensional Tectonics and Stratigraphy of the North Atlantic Margins. American Association of Petroleum Geologists, Memoir, 46, pp. 599–614.

Valencia-Moreno, M., Ruiz, J., Ochoa-Landin, L., Martínez-Serrano, R., Vargas-Navarro, P., 2003. Geochemistry of the Coastal Sonora batholith, northwestern Mexico. Canadian Journal of Earth Sciences 40, 819–831.

Varela, R., Dalla Salda, L., Cingolani, C., Gómez, V., 1991. Estructura, petrología y geocronología del basamento de la región de Limay, provincias de Río Negro y Neuquén, Argentina. Revista Geológica de Chile 18 (2), 147–163.

Varela, R., Basei, M.A.S., Cingolani, C.A., Siga, J.R.O., Passarelli, C.R., 2005. El basamento cristalino de las Andes norpatagónicos en Argentina: geocronología e interpretación tectónica. Revista geológica de Chile 32 (2), 167–187.

Vogt, K., Gerya, T., Castro, A., 2009. Modelling of silicic intrusions in Alpine type orogens. Eos 90, 29, Eos, Vol. 90, Number 52, 29 December 2009, Fall Meet. Suppl., Abstract p. 178.

Walker, J.D., Geiissman, J.W., 2009. Geologic Time Scale: Geological Society of America, doi: 10.1130/2009.CTS004R2C. The Geological Society of America.

Williams, L.S., 1998. U–Th–Pb geochronology by ion microprobe. In: McKibben, M.A., Shanks, W.C., Ridley, W.I. (Eds.), Applications of Microanalytical Techniques to Understanding Mineralizing Processes. Reviews in Economic Geology, 7, pp. 1–35.

Wyllie, P.J., 1977. From crucibles through subduction to batholiths. In: Saxena, S.K., Bhattacharja, S. (Eds.), Energetics of Geological Processes. Springer Verlag, pp. 389–433.

Zonenshayn, L.P., Savostin, L., Sedov, A., 1984. Global paleogeodynamic reconstruction for the last 160 million years. Geotectonics 18, 181–195.

Please cite this article in press as: Castro, A., et al., Petrology and SHRIMP U–Pb zircon geochronology of Cordilleran granitoids of the Bariloche area, Argentina, Journal of South American Earth Sciences (2011), doi:10.1016/j.jsames.2011.03.011